Ionization at a solid-water interface in an applied electric field: Charge regulation

Ryuichi Okamoto[1] and Akira Onuki[2]
[1]*Department of chemistry, Tokyo Metropolitan University, Hachioji, Tokyo 192-0397, Japan*
[2]*Department of Physics, Kyoto University, Kyoto 606-8502, Japan*
(Dated: August 17, 2016)

We investigate ionization at a solid-water interface in applied electric field. We attach an electrode to a dielectric film bearing silanol or carboxyl groups with an areal density Γ_0, where the degree of dissociation α is determined by the proton density in water close to the film. We show how α depends on the density n_0 of NaOH in water and the surface charge density σ_m on the electrode. For $\sigma_m > 0$, the protons are expelled away from the film, leading to an increase in α. In particular, in the range $0 < \sigma_m < e\Gamma_0$, self-regulation occurs to realize $\alpha \cong \sigma_m/e\Gamma_0$ for $n_0 \ll n_c$, where n_c is 0.01 mol/L for silica surfaces and is 2×10^{-5} mol/L for carboxyl-bearing surfaces. We also examine the charge regulation with decreasing the cell thickness H below the Debye length κ^{-1}, where a crossover occurs at the Gouy-Chapman length. In particular, when $\sigma_m \sim e\Gamma_0$ and $H \ll \kappa^{-1}$, the surface charges remain only partially screened by ions, leading to an electric field in the interior.

arXiv:1608.04462v1 [cond-mat.soft] 16 Aug 2016

I. INTRODUCTION

Numerous papers have been written on various aspects of the electric double layer at a solid-water interface[1–4]. However, not enough attention has yet been paid on physics and chemistry of ionizable solid surfaces in contact with an aqueous electrolyte solution. As a well-known example[1–10], silanol groups SiOH on a silica oxide surface at a density Γ_0 dissociate into SiO^- and mobile protons H^+. The surface charge density is $-e\Gamma_0\alpha$, where α is the degree of dissociation. In this case, α is determined by the proton density $n_{\rm H}(0)$ in water immediately close to the surface. This $n_{\rm H}(0)$ is different from the bulk proton density $n^0_{\rm H}$, depending on the solution composition. Also when two ionizable surfaces approach, α and the force between them change at small separation[1,11–16]. These behaviors are often referred to as *charge regulation*. We note that similar phenomena with variable charges are ubiquitous in soft matters.

We mention theoretical papers on the charge regulation on solid-water interfaces with salts[14–22]. Ninham and Parsegian[15] first presented a model of surface ionization using the mass action law as the boundary condition of the Poisson-Boltzmann (PB) equation, where Γ_0 and the dissociation constant K_s are relevant parameters. They determined α, the charge distribution, and the electric potential self-consistently. Behrens *et al.*[17–19] solved these equations accounting for a potential drop across the Stern layer formed on a solid surface in water. These theories are based on one-dimensional (1D) calculations of the PB solutions for symmetric ionizable surfaces. Behrens *et al.* also devised a formula for ionization of large colloidal particles.

In this paper, we construct a free energy functional for the ion densities n_i and α in applied field, accounting for the chemical reactions in the bulk and on the surface. We then examine the effect of sodium hydroxide NaOH at a low density n_0, where the hydroxyl density $n_{\rm OH}$ and the proton density $n_{\rm H}$ are related by the dissociation law $n_{\rm OH}n_{\rm H} = 10^{-14}$ mol^2/L^2 in bulk water[23]. Thus, adding NaOH serves to decrease $n_{\rm H}(0)$ and increase α. In experiments, the surface ionization due to deprotonation increased with addition of OH^- (with increasing pH)[14,24–27]. We also apply an electric field to the system attaching a planar electrode with a surface charge density σ_m. Then, there arises another kind of charge regulation. We assume that the electric double layer next to the film is determined by the effective density $\sigma_{\rm eff} = -e\Gamma_0\alpha + \sigma_m$. Thus, if σ_m is positive (negative), the cations including the protons tend to be repelled from (attracted to) the film, leading to an increase (a decrease) in α. We have $\alpha \to 0$ for $\sigma_m < 0$ and $\alpha \to 1$ for $\sigma_m > e\Gamma_0$. However, in the range $0 < \sigma_m < e\Gamma_0$, marked *self-regulation* behavior emeges, where α approaches $\sigma_m/e\Gamma_0$ and $\sigma_{\rm eff}$ nearly vanishes. In this effect, the NaOH density n_0 needs to be smaller than a characteristic density n_c, where n_c is much larger than the hydroxyl density 10^{-7} mol/L in pure water. For small wall separation H and for not small σ_m, screening of the surface charges can only be partial, leading to a negative disjoining pressure Π_d with large amplitude. For sufficiently large n_0 with small H, screening can also be achieved leading to a large positive Π_d. In this paper, we are in the nonlinear PB regime with addition of NaOH only, where the Debye length is longer than the Gouy-Chapman length[28].

Furthermore, in a mixture solvent, the dissociation on solid surfaces can strongly depend on the local solvent composition ϕ as well as the solvation of ions in the bulk[29]. In our previous paper[30], small variations of ϕ around the colloid surfaces induced significant changes in α and the ion distribution. Thus, there can be a strong coupling between ϕ and the ionization in mixture solvents, which alters adsorption and wetting on the surfaces and the interaction among the colloidal particles.

In polyelectrolytes and charged gels[31–38], the dissociation on polymer chains is governed by the local environments and is highly fluctuating in space and time. This can strongly affect coil-globule transition and phase separation, particularly when a second fluid component (cosolvent) is added to a water-like solvent. A first order phase transition of weak-to-strong ionization was also predicted on ionizable rods in a mixture solvent[34]. In

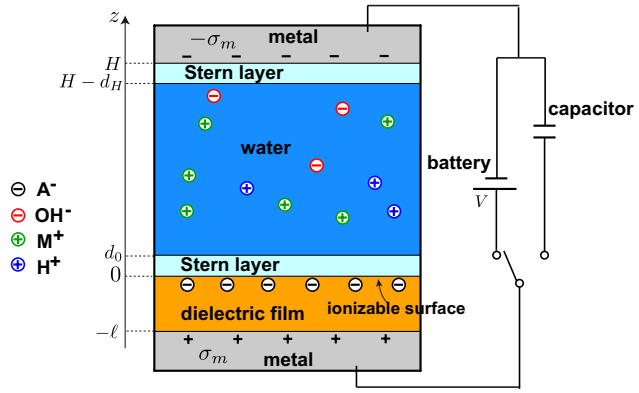

FIG. 1: Illustration of geometry. Two parallel metallic plates are placed at bottom ($z < -\ell$) and top ($z > H$) with charge densities $\pm\sigma_m$ and a potential difference V. A dielectric film with thickness ℓ is on the bottom metallic plate ($-\ell < z < 0$). At $z = 0$, ionizable groups AH with a density Γ_0 dissociate into A^- and H^+ with a fraction α. Water molecules are under strong influence of the walls in Stern layers ($0 < z < d_0$ and $H - d_H < z < H$). Protons also come from dissociation of water. MOH dissociates into M^+ and OH^-. If a battery is connected, V can be controlled, where the metal surface chage density σ_m fluctuates. If it is disconnected, σ_m becomes fixed. Furthermore, if a small capacitor is connected, σ_m can be changed by a small fixed amount (see Appendix A).

phase separation, α can be very different in the two phases[35–37]. With addition of alcohol to water, precipitation of DNA has also been observed[39], where ionization of DNA is favored in water-rich environments.

The organization of this paper is as follows. In Sec.II, we will present a coarse-grained Ginzburg-Landau free energy functional, which includes the electrostatic contributions from the Stern layers and the dielectric film. In Sec.III, we will present numerical results for silica-water interfaces for thick cells. In Sec.IV, we will discuss the ionization on carboxyl-bearing surfaces. In Sec.V, we will present results for thin cells.

II. THEORETICAL BACKGROUND

We illustrate our system in Fig.1, where a cell contains liquid water and ions in ambient conditions ($T = 300$ K and $p = 1$ atm) in the region $0 < z < H$ and a dielectric film is in the region $-\ell < z < 0$. For example, we suppose a ultra-thin silica oxide film with silanol groups in water. To apply electric field to the system, we place metallic walls at the two ends in the regions $z < -\ell$ and $z > H$. In our theory, we can fix the applied potential difference V or the electrode surface-change density σ_m.

The cell lengths in the lateral directions are much longer than H such that the edge effect is negligible. All the physical quantities are coarse-grained smooth variables depending only on z. Hereafter, the Boltzmann constant will be set equal to 1.

A. Chemical reactions in bulk and on surface

In the cell, we initially add a base MOH at a low density[26]. It dissociates into mobile univalent cations M^+ and hydroxide anions OH^- as

$$\mathrm{MOH} \rightleftarrows \mathrm{M}^+ + \mathrm{OH}^-. \tag{1}$$

In addition, a very small fraction of water molecules dissociate into H^+ and OH^- as[23]

$$\mathrm{H_2O} \rightleftarrows \mathrm{H}^+ + \mathrm{OH}^-. \tag{2}$$

We use the notation H^+, though the protons exist as hydronium ions H_3O^+ in liquid water. The local number densities of MOH, M^+, OH^-, and H^+ are written as $n_{\mathrm{MOH}}(z)$, $n_{\mathrm{M}}(z)$, $n_{\mathrm{OH}}(z)$, and $n_{\mathrm{H}}(z)$, respectively, which are coarse-grained smooth functions of z in our theory. The charge density $\rho(z)$ is written as

$$\rho = e(n_{\mathrm{H}} + n_{\mathrm{M}} - n_{\mathrm{OH}}). \tag{3}$$

In chemical equilibrium, the mass action laws hold:

$$n_{\mathrm{M}} n_{\mathrm{OH}}/n_{\mathrm{MOH}} = K_{\mathrm{b}}, \tag{4}$$
$$n_{\mathrm{OH}} n_{\mathrm{H}} = K_{\mathrm{w}}, \tag{5}$$

where K_{b} and K_{w} are the dissociation constants. For NaOH, we have $K_{\mathrm{b}} = 10^{-1}$mol/L$= 0.06$ nm^{-3}. However, $K_{\mathrm{w}}^{1/2}$ is much smaller ($= 10^{-7}$mol/L$= 6 \times 10^{-8}$/nm^3).

In a thick cell, a homogeneous bulk region appears far from the walls, where n_i assume bulk values, written as n_i^0. They satisfy Eqs.(4) and (5) and the charge neutrality condition $n_{\mathrm{M}}^0 + n_{\mathrm{H}}^0 = n_{\mathrm{OH}}^0$. We introduce the bulk density of M atoms by

$$n_0 = n_{\mathrm{M}}^0 + n_{\mathrm{MOH}}^0. \tag{6}$$

See Fig.2(a) for n_i^0 vs n_0 for M=Na. For such a strong base with large K_{b}, we can well assume $n_0 \ll K_{\mathrm{b}}$ to find

$$n_{\mathrm{M}}^0 \cong n_0, \quad n_{\mathrm{MOH}}^0 \cong n_{\mathrm{OH}}^0 n_0/K_{\mathrm{b}} \ll n_0, \tag{7}$$

where $n_{\mathrm{OH}}^0 \ll K_{\mathrm{b}}$. From $n_0 = (1 + n_{\mathrm{OH}}^0/K_{\mathrm{b}})(n_{\mathrm{OH}}^0 - n_{\mathrm{H}}^0)$, we can express n_0 in terms of n_{OH}^0 as

$$n_0 \cong n_{\mathrm{OH}}^0 - n_{\mathrm{H}}^0 = n_{\mathrm{OH}}^0 - K_{\mathrm{w}}/n_{\mathrm{OH}}^0, \tag{8}$$

In pure water, we have $n_0 = 0$ and $n_{\mathrm{OH}}^0 = n_{\mathrm{H}}^0 = K_{\mathrm{w}}^{1/2}$. For $n_0 \gg K_{\mathrm{w}}^{1/2}$, we obtain $n_{\mathrm{OH}}^0 \cong n_0$ and $n_{\mathrm{H}}^0 \cong K_{\mathrm{w}}/n_0 \ll K_{\mathrm{w}}^{1/2}$. In the following figures, supposing a strong base, we will use n_0 to represent the amount of the added base. However, our theoretical results will be expressed in terms of n_{OH}^0 and n_{H}^0 and will be valid for arbitrary K_{b}. In our figures Eq.(8) holds, so they can be used even for weak bases[27] if n_0 is related to n_{OH}^0 by Eq.(8)

On the surface of the dielectric film at $z = 0$, ionizable groups AH are distributed with a surface density Γ_0. No

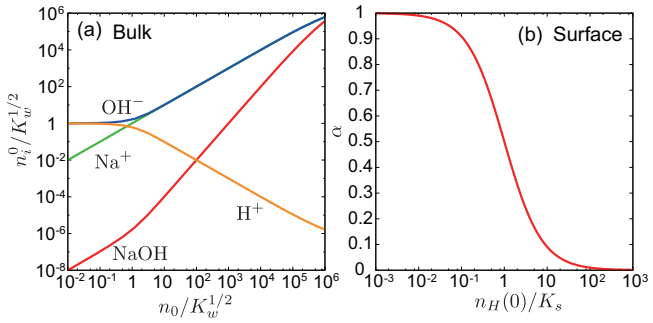

FIG. 2: Chemical reactions in this paper. (a) Equilibrium bulk densities n_i^0 (i = NaOH, Na^+, OH^-, and H^+) divided by $K_w^{1/2}$ vs $n_0/K_w^{1/2}$, where n_0 is the bulk density of Na atoms. (b) Equilibrium α vs $n_H(0)/K_s$ from Eq.(11).

dissociation is assumed on the upper metal surface. Depending on the local pH near the surface, a fraction α ($0 < \alpha < 1$) of these groups dissociate as[15]

$$\mathrm{AH} \rightleftarrows \mathrm{A}^- + \mathrm{H}^+. \tag{9}$$

Here, A^- anions remain on the surface $z = 0$, while the dissociated protons are mobile in water. The surface charge density due to A^- at $z = 0$ is

$$\sigma_A = -e\Gamma_0\alpha. \tag{10}$$

Let $n_H(0)$ be the proton density immediately close to the dielectric film in water. Then, the surface mass action law in chemical equilibrium is expressed as[15]

$$n_H(0)\alpha/(1-\alpha) = K_s, \tag{11}$$

where K_s is the surface dissociation constant. See Fig.2b for α vs $n_H(0)/K_s$. Since $\alpha = 1/[1 + n_H(0)/K_s]$, α tends to 1 (to 0) if $n_H(0)$ is much smaller (larger) than K_s.

We define the particle numbers $N_i = \int_0^H dz n_i(z)$ (i= MOH, M, OH, H) per unit area in the cell. Since the hydroxide and proton numbers due to the autoionization coincide, we have

$$N_{OH} - N_M = N_H - \Gamma_0\alpha. \tag{12}$$

It follows the overall charge neutrality condition,

$$\int_0^H dz\rho(z) + \sigma_A = 0. \tag{13}$$

In our theory, a reservoir can be attached or the system can be closed. In the latter case, the total number of the M atoms is fixed as

$$N_M + N_{MOH} = H\bar{n}, \tag{14}$$

where $\bar{n}$ is the initial density of the added base.

In Sec.III, we consider silica oxide surfaces with silanol groups AH= SiOH and set[5–8,14,17,19]

$$\begin{aligned} K_s &= 10^{-7.3}\mathrm{mol/L} = 3.0\times10^{-8}/\mathrm{nm}^3, \\ \Gamma_0 &= 8.0/\mathrm{nm}^2 \quad \text{(silica surface)}, \end{aligned} \tag{15}$$

where K_s is very small ($= 0.5K_w^{1/2}$). The pH and pK values are defined by $n_H^0 = 10^{-\mathrm{pH}}$ mol/L (in the bulk region) and $K_s = 10^{-\mathrm{pK}}$ mol/L. Then, pK= 7.3, $n_H^0/K_s = 10^{7.3-\mathrm{pH}}$, and $n_{OH}^0/K_s = 10^{\mathrm{pH}-6.7}$ here. The value of Γ_0 in Eq.(15) is obtained for nonporous, fully hydrated silica, so it is large. Experimental values of Γ_0 strongly depend on surface preparation[19]. It is also known that the adsorption $SiOH+H^+ \rightleftarrows SiOH_2^+$ takes place in high acidity (low pH) conditions[5,7], leading to a zero-charge surface state at a pH about 2. See Sec.IV for analysis on ionization on carboxyl-bearing surfaces.

B. Electric potential and Stern layers

As the electrostatic boundary condition, we may fix the potential difference between the electrodes:

$$V = \Phi(0) - \Phi(H) + \sigma_m/C_d. \tag{16}$$

We may also fix the surface charge density σ_m on the lower metal surface at $z = -\ell$ (see Appendix A). In the dielectric film, the electric field is given by $4\pi\sigma_m/\varepsilon_d$, where ε_d is the film dielectric constant. This yields the potential change $\Phi(-\ell) - \Phi(0) = \sigma_m/C_d$, where the film capacitance per unit area is written as

$$C_d = \varepsilon_d/4\pi\ell. \tag{17}$$

In the cell outside microscopic Stern layers (see below), $\Phi(z)$ obeys the Poisson equation,

$$-\varepsilon_0 d^2\Phi/dz^2 = 4\pi\rho, \tag{18}$$

where ε_0 is the solvent dielectric constant. The electric field is given by $E = -d\Phi/dz$.

Generally, the electric potential can change noticeably across a microscopic Stern layer at a solid-water interface[1–3,40]. We mention molecular dynamics simulations on this effect[41–45]. In our case, there are two such layers at the bottom and top. For simplicity, we assume no specific ion adsorption. Then, the ion amounts in the layers are negligibly small for small bulk ion densities[17–19,43]. Denoting the layer thickness as d_0 at $z = 0$ and as d_H at $z = H$, we assume linear relations,

$$\begin{aligned} V_0^S &= \Phi(0) - \Phi(d_0) = (\sigma_m + \sigma_A)/C_0, \\ V_H^S &= \Phi(H - d_H) - \Phi(H) = \sigma_m/C_H. \end{aligned} \tag{19}$$

For simplicity, the surface capacitances C_0 and C_H are taken to be those in the limit of small ion densities. Here, we can define the polarization $P(z)$ microscopically such that the electric induction $D(z) = E(z) + 4\pi P(z)$ is continuous through the layers[45], where $E(z)$ and $P(z)$ change abruptly in the layers[46]. We write $D(z)$ at the bottom and the top as

$$\begin{aligned} &D(d_0) = \varepsilon_0 E(d_0) = 4\pi(\sigma_A + \sigma_m). \\ &D(H - d_H) = \varepsilon_0 E(H - d_H) = 4\pi\sigma_m, \end{aligned} \tag{20}$$

These constitute the boundary conditions of the Poisson equation (18). The effective surface charge density is $\sigma_{\rm eff} = \sigma_{\rm A}+\sigma_m$ at the bottom. Furthermore, even without applied field ($\sigma_m = 0$), the previous simulations[41–45] have shown the presence of small potential drops at solid-water interfaces due to the anisotropy of water molecules . We neglect this intrinsic, surface effect in this paper.

The total potential difference V is now written as

$$V = [\Phi(d_0) - \Phi(H - d_H)] + \frac{\sigma_{\rm A} + \sigma_m}{C_0} + \frac{\sigma_m}{C'}, \qquad (21)$$

where the first term arises from the mobile ions and

$$C' = (1/C_H + 1/C_d)^{-1}. \qquad (22)$$

If we neglect the image interaction[48], the electrostatic free energy F_e appropriate at fixed σ_m is the space integral of $DE/8\pi$ in the whole region ($-\ell < z < H$). Then,

$$\begin{aligned} F_e &= \int_{d_0}^{H-d_H} dz \frac{\varepsilon_0 E^2}{8\pi} + \frac{(\sigma_A + \sigma_m)^2}{2C_0} + \frac{\sigma_m^2}{2C'} \\ &= \frac{1}{2}\int_0^H dz \rho\Phi + \frac{1}{2}\sigma_{\rm A}\Phi(0) + \frac{1}{2}\sigma_m V. \end{aligned} \qquad (23)$$

We rewrite the integral in the first line as $[\Phi(d_0)D(d_0) - \Phi(H-d_0)D(H-d_0)]/8\pi + \int dz\Phi\rho/2$ and use Eq.(20). It then follows the second line, where the integration region $d_0 < z < H - d_H$ has been changed to $0 < z < H$ and $\sigma_{\rm A}$ is related to ρ by Eq.(13). Note that the integrals of ρ in the Stern layers are assumed to be negligible.

We also consider small changes $\rho \to \rho + \delta\rho$ and $\sigma_m \to \sigma_m + \delta\sigma_m$. The incremental change in F_e is written as

$$\delta F_e = \int_0^H dz \Phi\delta\rho + \Phi(0)\delta\sigma_A + V\delta\sigma_m, \qquad (24)$$

where $\delta\sigma_A = -\int_0^H dz\delta\rho(z)$ from Eq.(13) and the last term vanishes at fixed σ_m. On the other hand, at fixed V, the appropriate free energy is $F_e - \sigma_m V$, whose differential form is given by the first two terms in Eq.(24). Here, we neglect the ion-ion correlation due to the fluctuations in the xy plane and the image interaction between the ions and the image charges in the solid regions.

In our analysis, we use the following capacitance values. (i) For our dielectric film, we assume $\varepsilon_d = 4$ and $\ell = 1.05$ nm to obtain $C_d = 0.0335$ F/m^2 from Eq.(17). On the other hand, in analysis of electrowetting, Klarman and Andelman[49] assumed a much smaller value, $C_d = 4.4 \times 10^{-6}$ F/m^2, for a film with $\varepsilon_d = 2.67$ and $\ell = 5$ μm. In their case, the relation $V \cong \sigma_m/C_d$ held nicely for not very small V. (ii) Supposing a silica-water interface[7,17–19], we set $C_0 = 2.9$ F/m^2. (iii) The metal-water capacitance[40,44] has been observed in the range $0.2-0.5$ F/m^2, so we set $C_H = 0.3$ F/m^2. Then, $1/C_H = 0.11/C_d$ in our case. Via microscopic simulations[41,44,45], the surface capacitance for a metal-water interface has been calculated in a range of $0.05-0.1$F/m^2 with a layer thickness about 5Å (where water molecules are depleted).

C. Free energy functional

We set up the Helmholtz free energy functional F for a cell with $d_0 \ll H$ and $d_H \ll H$ in the mean field theory. At fixed σ_m, it consists of three parts as

$$F = F_e + F_b + F_s. \qquad (25)$$

At fixed V, we should replace F_e by $F_e - \sigma_m V$. Here, F_b is the contribution from the solute particles and F_s is that for the surface ionization:

$$\begin{aligned} F_b/T &= \int_0^H dz \Big[\sum_i n_i[\ln(n_i\lambda_i^3) - 1] + \Delta_{\rm b} n_{\rm M} \\ &\qquad + \Delta_{\rm w}(n_{\rm OH} - n_{\rm M}) \Big], \end{aligned} \qquad (26)$$

$$F_s/T\Gamma_0 = \alpha\ln\alpha + (1-\alpha)\ln(1-\alpha) + \Delta_\sigma\alpha, \qquad (27)$$

where $\lambda_i (\propto T^{1/2})$ is the thermal de Broglie length of the particle species i. The $T\Delta_{\rm b}$, $T\Delta_{\rm w}$, and $T\Delta_s$ are the dissociation free energies for the chemical reactions in Eqs.(1), (2), and (9), respectively, which arise from the microscopic interactions. The above form of F_s has long been used in the literature[30–32,35,36,47], where the first two terms are entropic contributions.

We define the chemical potentials of the solute particles by $\mu_i = \delta F/\delta n_i$ at fixed α. Then, Eqs.(25)-(27) give

$$\mu_{\rm MOH}/T = \ln[n_{\rm MOH}\lambda_{\rm MOH}^3], \qquad (28)$$

$$\mu_{\rm M}/T = \ln[n_{\rm M}\lambda_{\rm M}^3] + \Delta_{\rm b} - \Delta_{\rm w} + U, \qquad (29)$$

$$\mu_{\rm OH}/T = \ln[n_{\rm OH}\lambda_{\rm OH}^3] + \Delta_{\rm w} - U, \qquad (30)$$

$$\mu_{\rm H}/T = \ln[n_{\rm H}\lambda_{\rm H}^3] + U, \qquad (31)$$

where $U(z) = e\Phi(z)/T$ is the normalized potential.

In equilibrium, we require the charge neutrality condition (12). Here, we can either assume Eq.(14) with a constant $\bar{n}$ in a closed cell or attach a reservoir to the cell with a common $\mu_{\rm MOH}$ (see Appendix B)[15]. In these cases, we should minimize the grand potential,

$$\begin{aligned} \Omega &= F - h_0(N_{\rm M} + N_{\rm MOH}) \\ &- h_1(N_{\rm H} - N_{\rm OH} + N_{\rm M} - \Gamma_0\alpha), \end{aligned} \qquad (32)$$

where h_0 and h_1 are homogeneous constants. Requiring $\delta\Omega/\delta n_i = 0$, we obtain the chemical equilibrium conditions for the mobile particles:

$$\mu_{\rm MOH} = \mu_{\rm M} + \mu_{\rm OH} = h_0, \qquad (33)$$

$$\mu_{\rm H} = -\mu_{\rm OH} = h_1. \qquad (34)$$

With these relations, Ω can be expressed as

$$\Omega = F - \sum_{i\neq{\rm H}} \mu_i N_i - \mu_{\rm H}(N_{\rm H} - \Gamma_0\alpha). \qquad (35)$$

See Appendix D for more detailed expressions of Ω.

Assuming the equilibrium conditions in Eqs.(33) and (34) for $n_i(z)$, we may treat $\Omega = \Omega(\alpha)$ as a function of

α. Then, its minimization with respect to α gives the equilibrium α. From Eq.(27) we obtain its derivative,

$$\frac{1}{T\Gamma_0}\frac{d\Omega}{d\alpha} = \ln(\frac{\alpha}{1-\alpha}) + \Delta_s + \ln[n_{\rm H}(0)\lambda_{\rm H}^3]. \tag{36}$$

Using Eqs.(33) and (34) and setting $d\Omega/d\alpha = 0$, we derive the chemical equilibrium conditions (4), (5), and (11) with the dissociation constants,

$$K_{\rm b} = (\lambda_{\rm MOH}/\lambda_{\rm H}\lambda_{\rm OH})^3 \exp(-\Delta_{\rm b}), \tag{37}$$
$$K_{\rm w} = (\lambda_{\rm H}\lambda_{\rm OH})^{-3} \exp(-\Delta_{\rm w}), \tag{38}$$
$$K_s = \lambda_{\rm H}^{-3} \exp(-\Delta_s). \tag{39}$$

With Eq.(39) the right hand side of Eq.(36) becomes $\ln[\alpha n_{\rm H}(0)/(1-\alpha)K_s]$, leading to Eq.(11) in equilibrium.

If we use K_b for NaOH and K_s for silica, Eqs.(37)-(39) give $\Delta_{\rm b} = 8.4$, $\Delta_{\rm w} = 51$, and $\Delta_s = 24$. These large sizes of $\Delta_{\rm w}$ and Δ_s indicate that the autoionization in water and the dissociation on a silica oxide surface are rare activation processes. On the other hand, $\Delta_{\rm b}$ is relatively small such that NaOH mostly dissociates in water.

We previously presented free energies with variable charges in mixture solvents for colloidal particles[30], rods[34], and polyelectrolytes[35] (without applied field). In such systems, if Δ_s depends on the composition, ionization and wetting transitions are coupled.

D. Space-dependence of ion densities

From Eqs.(28)-(31), $n_{\rm MOH}$ is a homogeneous constant. The ion densities can be expressed in terms of $U(z)$ as

$$n_{\rm OH}(z) = n_{\rm OH}^0 e^{U(z)}, \quad n_{\rm H}(z) = n_{\rm H}^0 e^{-U(z)},$$
$$n_{\rm M}(z) = n_{\rm M}^0 e^{-U(z)}. \tag{40}$$

where n_i^0 are constants with $n_{\rm M}^0 + n_{\rm H}^0 = n_{\rm OH}^0$. See Appendix B for more details on these expressions. From Eq.(18) we obtain the PB equation,

$$d^2U/dz^2 = \kappa^2 \sinh(U), \tag{41}$$

We define the Debye wave number κ by

$$\kappa = (8\pi\ell_B n_{\rm OH}^0)^{1/2} = 10^{-3}(n_{\rm OH}^0/K_{\rm w}^{1/2})^{1/2}/{\rm nm}. \tag{42}$$

where $\ell_B = e^2/\varepsilon_0 T = 7.0$ Å is the Bjerrum length. The inverse κ^{-1} is the Debye length, which is long here, but it can be shortened if we add a salt such as KCl. In such cases, $n_{\rm OH}^0$ in Eq.(42) should be replaced by the total anion density $n_{\rm b}^0$ in the bulk.

For $\kappa H \gg 1$, n_i^0 are the bulk ion densities far from the walls as in Eqs.(6)-(8), where the charge neutrality condition holds. However, even for not large κH, we can use Eq.(40) with well-defined n_i^0. Under Eq.(14) in a closed cell, $n_{\rm M}^0$ is determined by $n_{\rm M}^0 \int_0^H dz e^{-U}/H + n_{\rm MOH} = \bar{n}$ (see Eq.(58)). If we attach a reservoir to the cell with a common $n_{\rm MOH}$, n_i^0 in Eq.(40) are simply equal to the ion densities in the reservoir (see Appendix B).

The protons are assumed to penetrate into the Stern layers. From Eq.(19) the ratio of its values at $z = 0$ and d_0 is given by the Boltzmann factor $\exp(-eV_0^{\rm S}/T)$, so

$$n_{\rm H}(0)/n_{\rm H}(d_0) = \exp[-e(\sigma_{\rm A} + \sigma_m)/C_0 T]. \tag{43}$$

This relation was proposed by Behrens *et al.*[17–19], but it should be checked with microscopic simulations.

E. Osmotic and disjoining pressures

In our system, the osmotic pressure Π is defined in the bulk region $d_0 < z < H - d_H$ and is given by[4]

$$\Pi = T\sum_i n_i(z) - \frac{\varepsilon_0}{8\pi}E(z)^2, \tag{44}$$

where the first term is the partial pressure of the solute particles and the second term is the zz component of the Maxwell stress tensor[48]. In equilibrium, Π is a constant independent of z. In fact, $d\Pi/dz = 0$ from Eqs.(18) and (40). Here, we assume $H > d_0 + d_H \sim 1$ nm.

Let us treat the equilibrium (minimum) value of Ω under Eqs.(11), (33), and (34) as a function of the cell width H in the fixed charge or the fixed potential condition. In Appendix C, we will derive the following relation,

$$\Pi = -\frac{\partial}{\partial H}\Omega. \tag{45}$$

A similar formula holds for the force between two colloidal particles with H being their separation distance[51]. As will be shown in Appendix C, Eq.(45) holds when $n_{\rm MOH}$ or $h_0 = \mu_{\rm MOH}$ in Eq.(33) is fixed in the derivative. This is equivalent to fixing $n_{\rm M} n_{\rm OH}$ from Eq.(4). It can be realized if we attach a reservoir to the cell. On the other hand, if the cell is closed and $\bar{n}$ in Eq.(14) is fixed, Eq.(C5) in Appendix C leads to $\Pi = -\partial F/\partial H$.

We suppose a reservoir without applied field. The $n_{\rm MOH}$ in the reservoir is the same as that in the cell. Then, the disjoining pressure is the difference $\Pi_d = \Pi - \Pi_r^0$, where Π_r^0 is the osmotic pressure in the reservoir (see Appendix B). Using $n_{\rm OH}^0$ in Eq.(40), we find[1,4,22]

$$\Pi_d = T n_{\rm OH}^0 [2\cosh(U) - 2 - \kappa^{-2}|dU/dz|^2]. \tag{46}$$

Thus, $\Pi_d = -\partial(\Omega + H\Pi_r^0)/\partial H$ at fixed $n_{\rm MOH}$. In the presence of other kinds of monovalent ions, $n_{\rm OH}^0$ in Eq.(46) should be replaced by the total anion (cation) density $n_{\rm b}^0$ in the reservoir, as stated below Eq.(42).

III. IONIZATION ON SILICA SURFACE AT LARGE WALL SEPARATION

We consider equilibrium in a thick cell with $H \gg \kappa^{-1}$, d_0, and d_H. In the middle region $z \gg \kappa^{-1}$ and $H - z \gg \kappa^{-1}$, the electrolyte is homogeneous with bulk ion densities n_i^0.

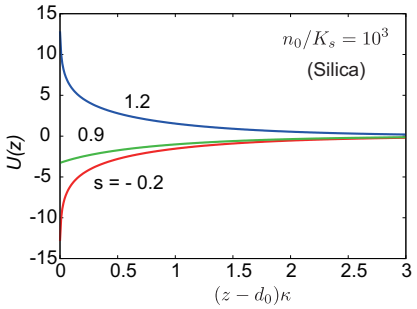

FIG. 3: Normalized electric potential $U(z)$ above the Stern layer ($z > d_0$) near the bottom wall at $A_1 = 1550$ ($n_0/K_s = 10^3$ for silica), where α depends on $s = \sigma_m/e\Gamma_0$. For three curves the initial slope at $z = d_0$ is $2A_1u$ with $u = \alpha - s$, where $(s, \alpha) = (-0.20, 2.2\times10^{-5})$, $(0.90, 0.902)$, and $(1.2, 1.0)$ from below. Thus, $u = 0.20$, 0.002, and -0.2, respectively. For the middle curve ($s = 0.90$), $0 < u \ll 1$ due to self-regulation. For the other curves the initial slope is steep.

A. Basic solution for large H

For $H \gg \kappa^{-1}$, we impose the semi-infinite boundary condition: $U(z) \to 0$ far from the walls. Near the bottom and the top, the profiles of the diffuse layers are given by

$$U(z) = 2\ln\left[\frac{1-\eta e^{-\kappa(z-d_0)}}{1+\eta e^{-\kappa(z-d_0)}}\right] \quad \text{(bottom)}$$
$$= 2\ln\left[\frac{1-\zeta e^{\kappa(z-H+d_H)}}{1+\zeta e^{\kappa(z-H+d_H)}}\right] \quad \text{(top)}. \tag{47}$$

From Eq.(20) the coefficients η and ζ are determined by

$$2\eta/(1-\eta^2) = -(2\pi\ell_B/e\kappa)(\sigma_{\rm A}+\sigma_m), \tag{48}$$
$$2\zeta/(1-\zeta^2) = (2\pi\ell_B/e\kappa)\sigma_m. \tag{49}$$

We define dimensionless parameters A_1, A_2, u, and s by

$$A_1 = 2\pi\ell_B\Gamma_0/\kappa = \Gamma_0(\pi\ell_B/2n^0_{\rm OH})^{1/2}, \tag{50}$$
$$A_2 = e^2\Gamma_0/C_0T, \tag{51}$$
$$u = -(\sigma_{\rm A}+\sigma_m)/e\Gamma_0 = \alpha - s, \tag{52}$$
$$s = \sigma_m/e\Gamma_0. \tag{53}$$

Then, the right hand side of Eq.(48) is A_1u and that of Eq.(49) is A_1s. From Eq.(20), dU/dz is $2A_1u$ at $z = d_0$ and is $-2A_1s$ at $z = H - d_H$ as the boundary conditions.

In terms of these parameters the total potential difference in Eq.(21) is rewritten as

$$\frac{e}{T}V = -g(A_1u) - A_2u + g(A_1s) + \frac{e\sigma_m}{TC'}. \tag{54}$$

where $g(x) = 2\ln[\sqrt{1+x^2}+x]$. Then, $g(-x) = -g(x)$. In Eq.(54) the first term ($= U(d_0)$) arises from the lower diffuse layer, the second from the lower Stern layer, the third ($= -U(H-d_H)$) from the upper diffuse layer, and the last term is due to the dielectric film and the upper Stern layer with Eq.(22). Here, the Debye-Hückel theory is valid only for $|u| \ll A_1^{-1}$ at the bottom and for $|s| \ll A_1^{-1}$ at the top. For silica, we have $A_1 = 4.9\times10^4(K_s/n^0_{\rm OH})^{1/2}$ and $A_2 = 17$. Thus, $A_1 \gg 1$ for realistic $n^0_{\rm OH}$ because of large Γ_0 and small κ.

Ninham and Parsegian[15] set pK=4.8, $\Gamma_0 = 1$ and $0.25/{\rm nm}^2$, and $\kappa = 1.29/{\rm nm}$ with a salt added. As a result, A_1 in Eq.(50) was of order 1 and κ^{-1} did not exceed the Gouy-Chapman length (see Eq.(56) below).

B. Profiles in the nonlinear PB regime

There appear three cases with increasing s: (i) $s < 0$ and $u > 0$ with $dU/dz > 0$, (ii) $s > 0$ and $u > 0$ with $U(z)$ lower near the walls than in the middle, and (iii) $s > 0$ and $u < 0$ with $dU/dz < 0$. We are interested in the nonlinear behavior of α in case (ii), since $\alpha \to 0$ in case (i) and $\alpha \to 1$ in case (iii).

In Fig.3, we display $U(z)$ near the bottom for $A_1 = 1.55\times10^3$ (at $n_0/K_s = 10^3$ for silica), where α is determined for given n_0 and s. Then, $(s, \alpha) = (-0.20, 2.2\times10^{-5})$, $(0.90, 0.902)$, and $(1.2, 1.0)$. In the case of $s = 0.9$, u is small ($= 0.002$) or $(\sigma_{\rm A}+\sigma_m)/\sigma_m \cong -0.002$, but $A_1u = 3.1$ in the nonlinear PB regime. We shall see that this charge cancellation is a universal effect.

Let us consider the profile of U and $n_{\rm H}$ at the bottom in the nonlinear PB regime $A_1u \gg 1$ with $u > 0$. The coefficient η in Eq.(48) is close to 1 as $\eta \cong 1 + 1/A_1u$, so

$$U(z) \cong 2\ln[(\kappa(z - d_0 + \ell_{\rm GC})/2],$$
$$n_{\rm H}(z)/n^0_{\rm H} \cong 4\kappa^{-2}(z - d_0 + \ell_{\rm GC})^{-2}. \tag{55}$$

Here, $\ell_{\rm GC}$ is the Gouy-Chapman length[28] at the bottom,

$$\ell_{\rm GC} = (\kappa A_1|u|)^{-1} = e/(2\pi\ell_B|\sigma_{\rm A}+\sigma_m|), \tag{56}$$

where we assume $\ell_{\rm GC} \ll \kappa^{-1}$. The profiles change on the scale of $\ell_{\rm GC}$. In this case, $n_{\rm H}(d_0)$ is larger than $n^0_{\rm H}$ as

$$n_{\rm H}(d_0)/n^0_{\rm H} \cong (2A_iu)^2. \tag{57}$$

The ratio $n_{\rm M}(d_0)/n^0_{\rm M}$ is also given by the right hand side of Eq.(57), which is important for $n^0_{\rm M} \cong n^0_{\rm OH} \gg n^0_{\rm H}$.

We also calculate the integral $N_{\rm H} = \int_o^H dz n_{\rm H}(z)$ using Eqs.(40) and (47). For $\kappa H \gg 1$, we thus obtain

$$N_{\rm H}/Hn^0_{\rm H} - 1 = 2A_1\alpha/\kappa H$$
$$+2[(A_1^2u^2+1)^{1/2} + (A_1^2s^2+1)^{1/2} - 2]/\kappa H. \tag{58}$$

The right hand side is the correction ($\propto H^{-1}$). It can also be equated with $N_{\rm M}/Hn^0_{\rm M} - 1$ for M^+ and $(N_{\rm OH} + \Gamma_0\alpha)/Hn^0_{\rm OH} - 1$ for OH^-, where $N_{\rm M}/H = \bar{n} - n_{\rm MOH}$ from Eq.(14) and $n^0_{\rm M} = n_0 - n_{\rm MOH}$ from Eq.(7). It follows $n^0_{\rm H} \le N_{\rm H}/H$ for any u and s. In particular, if $u \gg A_1^{-1}$ and $s \gg A_1^{-1}$, the right hand side is $4A_1\alpha/\kappa H$ and is negligible only for $H \gg A_1\alpha\kappa^{-1}$. Thus, for $\kappa H < A_1\alpha$, the ion densities N_i/H and n^0_i are largely different.

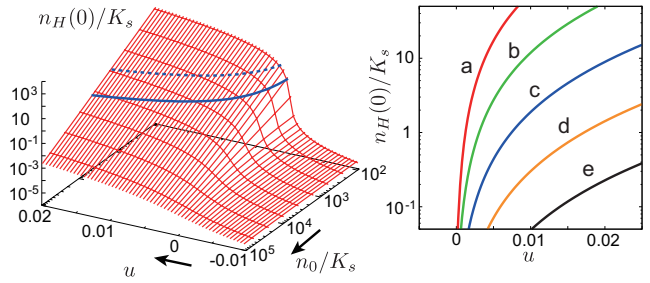

FIG. 4: Left: Ratio $n_{\rm H}(0)/K_s$ from Eq.(59) in the u-n_0/K_s plane with u in Eq.(52), which is $(1-\alpha)/\alpha$ in equilibrium. On the surface, it is 1 on the lower bold line and is 10 on the upper dotted line, where α is 0.5 and 0.09, respectively . Right: $n_{\rm H}(0)/K_s$ vs u with n_0/K_s being (a) 2.5×10^2, (b) 6.3×10^2, (c) 1.6×10^3 (right), (d) 4.0×10^3, and (e) 1.0×10^4 from above, where increase is steep for $n_0/K_s<10^{-4}$.

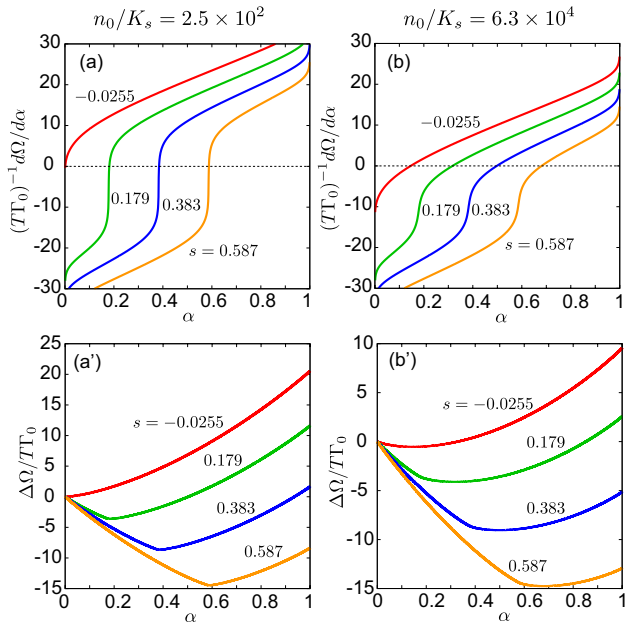

FIG. 5: Left: $d\Omega(\alpha)/d\alpha$ and $\Delta\Omega=\Omega(\alpha)-\Omega(0)$ divided by $T\Gamma_0$ as functions of α for $s=\sigma_m/e\Gamma_0=-0.0255, 0.179, 0.383$, and 0.587 at $n_0/K_s=2.5\times10^2$. Minimization of $\Omega(\alpha)$ gives equilibrium α. Right: those at $n_0/K_s=6.3\times10^4$.

C. Numerical results on α

Use of Eqs.(40) and (43) gives the ratio of the surface proton density $n_{\rm H}(0)$ to the bulk one $n_{\rm H}^0$ as

$$n_{\rm H}(0)/n_{\rm H}^0=\exp[g(A_1u)+A_2u] \\ =[(1+A_1^2u^2)^{1/2}+A_1u]^2e^{A_2u}, \qquad (59)$$

which depends on u and n_0. The right hand side increases with increasing u being equal to 1 for $u=0$. In Eq,(52), $-u$ denotes the normalized, effective surface charge density at $z=0$. Thus, for $u>0$ ($u<0$), the protons are more enriched (decreased) near the surface than in the bulk. From $A_1\gg1$, $n_{\rm H}(0)/n_{\rm H}^0$ can be of order only in the narrow range $|u|<A_1^{-1}$. Outside this range, it grows or decays rapidly depending on the sign of u as

$$n_{\rm H}(0)/n_{\rm H}^0\cong(2A_1u)^2e^{A_2u}\gg1 \qquad (u\gg A_1^{-1}) \\ \cong(2A_1|u|)^{-2}e^{-A_2|u|}\ll1 \quad (-u\gg A_1^{-1}). \qquad (60)$$

These changes occur in the region $z<\ell_{\rm GC}$ (see Eq.(57)).

In the surface chemical equilibrium (11), relevant is the ratio $n_{\rm H}(0)/K_s$, which is close to $(K_{\rm w}/K_sn_{\rm OH}^0)(n_{\rm H}(0)/n_{\rm H}^0)$ and is calculated from Eq.(59). In the left panel of Fig.4, it is plotted in the u-n_0/K_s plane. From Eq.(60), it grows abruptly from small values ($\ll1$) to large values ($\gg1$) with increasing u above 0. In the right panel, we show curves of $n_{\rm H}(0)/K_s$ vs u for several n_0/K_s, for which A_1 is indeed large (2.5×10^3 for curve (a) and 3.9×10^2 for curve (e)). For each point on the surface or the curves in Fig.4 we can find the corresponding equilibrium by setting $\alpha=[1+n_{\rm H}(0)/K_s]^{-1}$ and $\sigma_m=e\Gamma_0(\alpha-u)$.

Substitution of Eq.(59) into Eq.(36) gives $d\Omega(\alpha)/d\alpha$ as a function of α for given σ_m and n_0. In Fig.5, we plot it

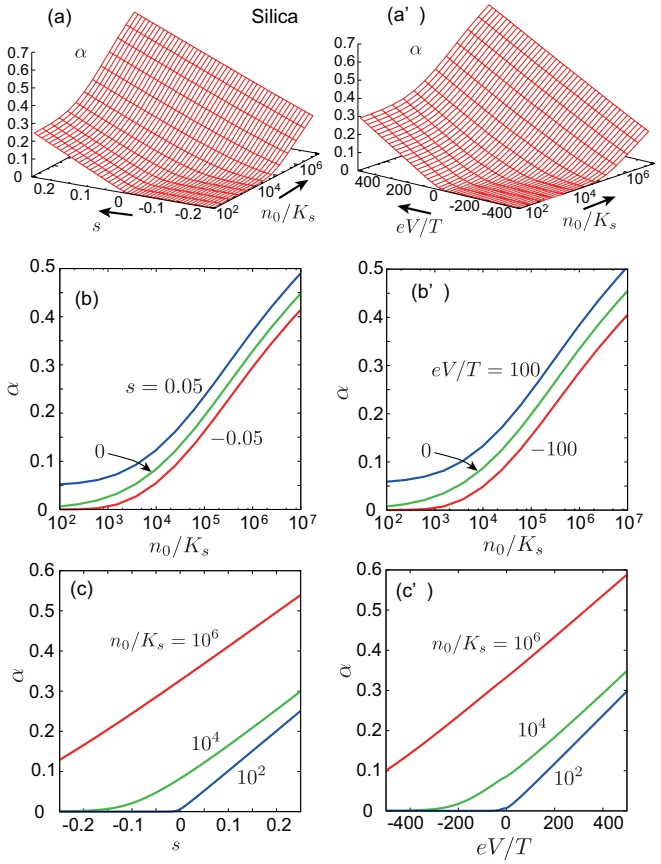

FIG. 6: Equilibrium α for silica in charge-controlled case (left) and in potential-controlled case (right). Top: α in the s-n_0/K_s plane in (a) and in the eV/T-n_0/K_s plane in (a'), where $s=\sigma_m/e\Gamma_0$. Middle: α vs n_0/K_s at $s=0$ and ±0.05 in (b) and $eV/T=0$ and ±100 in (b'), where $n_0/K_s=10^{\rm pH-6.7}$ in terms of the bulk pH. Bottom: α vs s in (c) and α vs eV/T in (c') for $n_0/K_s=10^2$, 10^4, and 10^6, which are nearly linear.

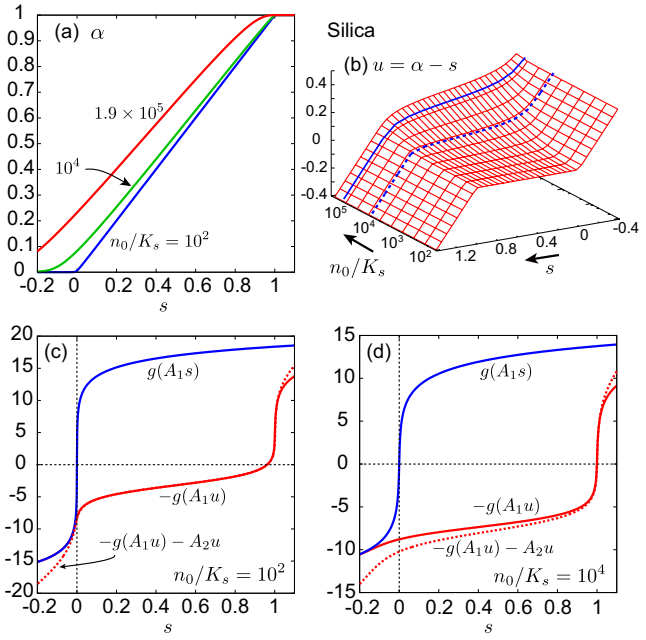

FIG. 7: (a) α vs $s=\sigma_m/e\Gamma_0$ for $n_0/K_s=10^2$, 10^4, and 1.9×10^5 in range $[-0.2,1.1]$ for silica, where $\alpha\cong s$. (b) $u=\alpha-s$ in the s-n_0/K_s plane, which is very small for $0<s<1$ and $n_0\ll n_c$. The lines (blue) on the surface indicate $n_0/n_c=0.1$ and 1. (c) Terms in eV/T in Eq.(54) for $n_0/K_s=10^2$: $g(A_1s)$ from the upper diffuse layer, $-g(A_1u)$ from the lower diffuse layer, and $-g(A_1u)-A_2u$ including the lower Stern layer contribution. (d) Those for $n_0/K_s=10^4$. In (c) and (d), the PB equation can be linearized only for $|g(A_1u)|<1$ at the bottom and $|g(A_1s)|<1$ at the top.

and its integral $\Delta\Omega=\int_0^\alpha d\alpha(d\Omega/d\alpha)=\Omega(\alpha)-\Omega(0)$ as functions of α for four $s=\sigma_m/e\Gamma_0$. See Appendix D for the explicit expression of $\Delta\Omega$. Minimization of $\Delta\Omega(\alpha)$ yields equilibrium α satisfying Eq.(11). For $n_0/K_s=2.5\times10^2$ (left), $d\Omega(\alpha)/d\alpha$ grows abruptly and $\Delta\Omega(\alpha)$ has a cusp-like minimum around $\alpha\cong s=\sigma_m/e\Gamma_0$ with $0<u\ll1$ (see Fig.7b). For a larger $n_0/K_s=6.3\times10^4$ (right), $d\Omega(\alpha)/d\alpha$ grows gradually and $\Delta\Omega(\alpha)$ has a broad minimum.

In Fig.6, we plot the equilibrium α as a function of σ_m and n_0 (left) and as a function of V and n_0 (right), where σ_m and V are related by Eq.(54). Salient results are as follows. (i) We can see close resemblance between the left and right panels, which suggests an approximate linear relation $V\propto\sigma_m$ (see Sec.IIID). In these panels, α increases with increasing n_0 in agreement with the experiment[24–26]. (ii) In the middle, we write α vs n_0/K_s, where we fix $s=\sigma_m/e\Gamma_0$ at 0 and ±0.05 in (b) and eV/T at 0 and ±100 in (b'). These curves exhibit different behaviors with a crossover at $n_0/K_s\sim10^4$. The curve of $\sigma_m=0$ exhibits the power-law behavior $\alpha\propto n_0^{2/3}$ for small n_0 (see Eq.(63)). (iii) In the bottom, at fixed n_0, we write α vs $s=\sigma_m/e\Gamma_0$ in (c) and α vs eV/T in (c'), where α increases linearly with increasing s or eV/T. See below for its explanation.

Note that the α-n_0 relation in the 1D geometry at $s=0$ can be used for colloidal particles with large radius ($\gg\kappa^{-1}$)[17–19]. At $\sigma_m=0$, Behrens and Grier[19] calculated the curves of α vs pH in agreement with Fig.6b. At the special point $\sigma_m=n_0=0$, we find $\alpha=4.7\times10^{-4}$ and $\sigma_A=-0.06$ μC/cm^2, where the latter is close to its experimental value -0.08 μC/cm^2 for silica colloidal particles in pure water[26].

D. Equation for α in nonlinear regime

In the nonlinear PB regime with $u=\alpha-s\gg A_1^{-1}$, Eqs.(11) and (60) give the following equation of α,

$$\begin{aligned}\alpha u^2e^{A_2u}/(1-\alpha) &= K_s\kappa^2/[(2\pi\ell_B\Gamma_0)^2n_H^0]\\ &= (n_{OH}^0/n_c)^2. \end{aligned}\tag{61}$$

In the second line, we set $\kappa^2/n_H^0=8\pi\ell_B(n_{OH}^0)^2/K_w$ and we introduce a crossover ion density n_c by

$$n_c=(2\pi\ell_BK_w/K_s)^{1/2}\Gamma_0.\tag{62}$$

For silica with NaOH, we find $n_c=0.97\times10^{-2}$mol/L $=1.9\times10^5K_s$ from Eq.(15). For surfaces with smaller pK (much larger K_s), we may add HCl to increase n_H^0 (instead of NaOH) at densities much larger than $K_w^{1/2}$; then, the right hand side of Eq.(61) becomes $K_w/n_c^2=K_s/[2\pi\ell_B\Gamma_0^2]$.

We note that Eq.(61) reproduces the curves of $|s|\ll1$ in Fig.6b, where we can see $\alpha\ll1$ for $n_0\ll n_c$. In particular, for $s=0$ and $n_0\ll n_c$, Eq.(61) gives

$$\alpha\cong\alpha_c=(n_{OH}^0/n_c)^{2/3}=\alpha_{c0}(n_{OH}^0/K_w^{1/2})^{2/3}.\tag{63}$$

In pure water, α_c tends to the following,

$$\alpha_{c0}=(K_w^{1/2}/n_c)^{2/3}=(K_s/2\pi\ell_B)^{1/3}/\Gamma_0^{2/3},\tag{64}$$

For silica, we find $\alpha_{c0}=4.7\times10^{-4}=5.4/A_1$ and $U(d_0)=-7.0$, so we are already in the nonlinear PB regime at $\sigma_m=n_0=0$. In terms of the bulk pH, we obtain $\log_{10}(\alpha/\alpha_{c0})=2(\text{pH}-7)/3$. Note that the relation (59) applies to large colloidal particles in the nonlinear PB regime. On the other hand, for $n_0>n_c$, u increases and the factor e^{A_2u} becomes important.

Let us assume $n_0\ll n_c$ for $n_c\gg K_w^{1/2}$. In Fig.7a, we confirm the behavior $\alpha\cong s$ in the range $0<s<1$, while we have $\alpha\cong0$ for $s<0$ and $\alpha\cong1$ for $s>1$. In (b), this behavior can be seen on a flat part of the surface of $u=\alpha-s$ in the s-n_0/K_s plane. Here, *self-regulated ionization* is realized, where the surface charge density σ_A due to deplotonation nearly cancels the applied surface charge density σ_m. To be more precise, Eq.(61) yields

$$u=\alpha-s\cong(1-s)^{1/2}s^{-1/2}n_{OH}^0/n_c\tag{65}$$

which is much smaller than $s(\cong\alpha)$ for $s\gg\alpha_c$ with α_c being defined by Eq.(63). If $|s|<\alpha_c$, α becomes of order

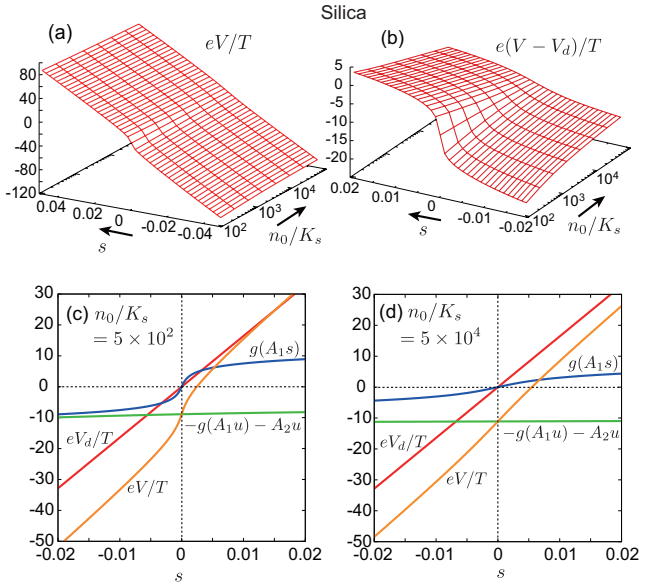

FIG. 8: Potential contributions in Eq.(54) (silica). Top: (a) eV/T ($|s|<0.05$) and (b) $e(V-V_d)/T$ ($|s|<0.02$) in the s-n_0/K_s plane, where $s=\sigma_m/e\Gamma_0$ and $V_d=\sigma_m/C'$. Bottom: Plotted are $-g(A_1u)-A_2u$, $g(A_1s)$, V_d, and their sum V as functions of s, where n_0/K_s is (c) 5×10^2 and (d) 5×10^4. See (c) and (d) of Fig.7 for expanded plots of $-g(A_1u)$, $-g(A_1u)-A_2u$, and $g(A_1s)$.

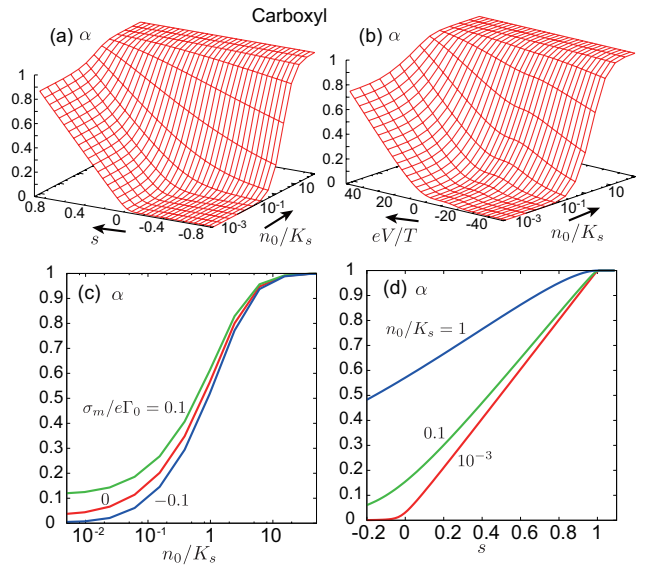

FIG. 9: Ionization on carboxyl-bearing surface. (a) α in the s-n_0/K_s plane and (b) α in the eV/T-n_0/K_s plane, where $s=\sigma_m/e\Gamma_0$. (c) α vs n_0/K_σ at $s=0$ and ±0.1. (d) α vs s for $n_0/K_s=10^{-3}$, 0.1, and 1 in range $[-0.2,1.1]$.

α_c, which is consistent with Eq.(63). On the other hand, if $n_c/K_{\rm w}^{1/2}$ is not large (with smaller $\Gamma_0/K_s^{1/2}$), u remains not small for any n_0.

Finally, we need to require $A_1u\gg1$ self-consistently, which has been assumed in setting up Eq.(61). For $|s|\gg\alpha_c$, use of Eqs.(50) and (64) gives

$$A_1u\cong(1-s)^{1/2}s^{-1/2}(n_{\rm OH}^0K_s/4K_{\rm w})^{1/2}. \tag{66}$$

If $n_{\rm OH}^0\gtrsim K_{\rm w}/K_s$, A_1u surely exceeds 1 for s not very close to 1, including the point $s=n_0=0$. Thus, it generally follows the self-regulation of surface ionization for $n_0\ll n_c$ and $0<\sigma_m<e\Gamma_0$.

E. Potential difference V between electrodes

In Appendix A, we will explain experimental setups at fixed V and σ_m, so we should compare the results from these two boundary conditions. So far we have found that the right and left panels in Fig.6 look similar.

In Eq.(54) the contributions to eV/T are written explicitly. In the bottom panels of Fig.7, we examine them in the range $-0.2<s=\sigma_m/e\Gamma_0<1.1$ as in the upper panels. Here, $g(A_1s)$ is from the upper diffuse layer, $-g(A_1u)$ is from the lower diffuse layer, and $-g(A_1u)-A_2u$ includes the lower Stern layer contribution, where n_0/K_s is 10^2 in (c) and 10^4 in (d). For positive s not close to 0, the contribution from the lower diffusive layer is smaller than that from the upper one in magnitude, which is consistent with Fig.7b. Here, for $u\gg A_1^{-1}$ and $s\gg A_1^{-1}$, we have $U(d_0)\cong-2\ln(2A_1u)$ and $U(H-d_H)\cong-2\ln(2A_1s)$. We are thus in the nonlinear PB regime for most s. The contribution $-A_2u$ from the lower Stern layer is appreciable for $s<0$ and $0<s\ll1$ or for $\alpha\ll1$.

In Fig.8, we display (a) eV/T and (b) $e(V-V_d)/T$ in the s-n_0/K_s plane with $V_d=\sigma_m/C'$, where the surfaces are rather flat for not very small s. We also compare eV/T, eV_d/T, $g(A_1s)$, and $-g(A_1u)-A_2u$ in the narrow range $|s|<0.02$ for $n_0/K_s=5\times10^2$ in (c) and 10^4 in (d). We recognize that V is close to V_d except for small σ_m even for our choice $\ell=1.05$ nm. With further increasing ℓ, the film contribution σ_m/C_d becomes more dominant in V, as in electrowetting experiments[49,50].

IV. IONIZATION ON CARBOXYL-BEARING SURFACE AT LARGE WALL SEPARATION

The carboxyl surface groups undergo the dissociation (COOH $\rightleftarrows$ COO$^-$ + H$^+$) at pK= 4.9 with a much smaller Γ_0 in water. In their analysis, Behrens *et al*[17–19] used two values, $\Gamma_0=0.574$ and 0.250 nm^{-2}, for carboxyl-bearing surfaces. These pK and Γ_0 are very different from those in Eq.(15) for silica. It is worth noting that Aoki *et al.*[52] fabricated a carboxyl functionalized latex film with coalescence of latex particles on a Pt electrode. Analysis has also been made on other surfaces such as iron oxide ones[14,17,19], which can be positively charged at low pH due to protonation.

In this section, we examine the equilibrium ionization on a carboxyl-bearing film in the 1D geometry in Fig.1

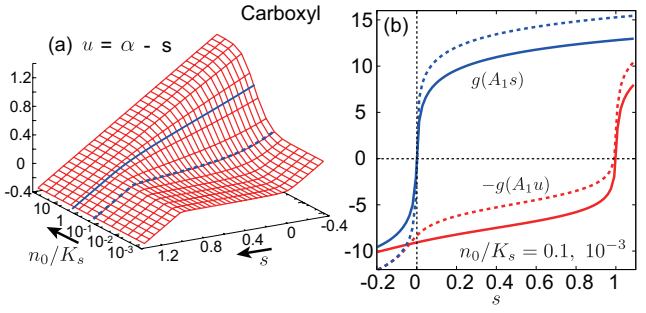

FIG. 10: (a) $u = \alpha - s$ in the s-n_0/K_s plane for carboxyl-bearing surface, which is very small for $0 < s < 1$ and $n_0 < 0.1n_c \sim K_s$. The lines (blue) on the surface indicate $n_0/n_c = 0.1$ and 1. (b) Terms in eV/T in Eq.(54): $g(A_1 s)$ from the upper diffuse layer and $-g(A_1 u)$ from the lower diffuse layer. for $n_0/K_s = 0.1$ (bold line) and 10^{-3} (dotted line).

with addition of NaOH in applied field. We set

$$K_s = 10^{-4.9}\text{mol/L} = 7.5 \times 10^{-6}/\text{nm}^3,$$
$$\Gamma_0 = 0, 25/\text{nm}^2 \quad (\text{carboxyl}-\text{bearing surface}). \tag{67}$$

Here, K_s is much larger than $K_{\rm w}^{1/2}$ by $10^{2.1} = 126$. According to Behrens *et al.*[17–19], the Stern capacitance at carboxyl-bearing surfaces is larger than that for silica oxide surfaces such that its presence itself can be neglected. In fact, for $C_0 = 10$ F/m^2, A_2 in Eq.(51) is of order 0.1 so $e^{A_2 u} \cong 1$ in Eq.(59) for $|u| \lesssim 1$. The other parameters are the same as in the silica case in Sec.III.

We use the PB theory in the previous section for large H. The parameter A_1 in Eq.(50) becomes $A_1 = 1.5 \times 10^3 (K_s/n_{\rm OH}^0)^{1/2}$. In Eq.(61) we neglect the Stern factor $e^{A_2 u}$ and assume $u = \alpha - s \gg A_1^{-1}$ to obtain

$$\alpha u^2/(1-\alpha) \cong (n_{\rm OH}^0/n_c)^2, \tag{68}$$

where $n_c = 1.9 \times 10^{-5}$mol/L $= 1.5 K_s$ from Eq.(67). It is smaller than that for silica by 500^{-1}. At the special point $n_0 = \sigma_m = 0$, our numerical analysis indicates $U(0) = -8.32$ and $\alpha_{c0} = 0.0a30 = 32/A_1$, where the latter nearly coincides with α_{c0} in Eq.(64). We are in the nonlinear PB regime at this point.

In Fig.9, we show α in (a) the s-n_0/K_s plane and in (b) the eV/T-n_0/K_s plane, as in (a) and (a') of Fig.6. Here, $\log_{10}(n_0/K_)$ = pH − 9.1. These look similar as in Fig.6, indicating the linear relation $V \cong \sigma/C'$ except for small σ_m. In (c), α vs n_0/K_s is plotted for $s = 0$ and ± 0.1, as in Fig.6b. Here, α approaches 1 for $n_0 \sim 6K_s \sim 4n_c$. The curve at $\sigma_m = 0$ coincides with that calculated by Behrens and Grier[19]. In (d), we display α vs s for $n_0/K_s = 10^{-3}$, 0.1, and 1 in the range $-0.2, s < 1.1$, as in Fig.7a. We can again find the linear behavior $\alpha \cong s$ for $0 < s < 1$ for $n_0 \ll n_c$.

In Fig.10, displayed is (a) $u = \alpha - s$ in the s-n_0/K_s plane for carboxyl-bearing surface, which is very small for $0 < s < 1$ and $n_0 < 0.1n_c \sim /K_s$, as in Fig.7b. The lines (blue) on the surface indicate $n_0/n_c = 0.1$ and 1. (b) Terms in eV/T in Eq.(54) for $n_0/K_s = 10^2$: $g(A_1 s)$ from the upper diffuse layer, $-g(A_1 u)$ from the lower diffuse layer. for $n_0/K_s = 0.1$ (bold line) and 10^{-3} (dotted line).

V. IONIZATION AND DISJOINING PRESSURE AT SMALL WALL SEPARATION

The disjoining pressure Π_d in Eq.(46) is a measurable qunatity[1,11–13]. It has been calculated between ionizable surfaces at small separation[15,16,22]. Here, attaching a reservoir, we examine how Π_d and α depend on H and σ_m with NaOH added at a density n_0. We consider the Stern layers, so we define the effective cell thickness by

$$H' = H - (d_0 + d_H), \tag{69}$$

where d_0 and d_H are of order 5Å. There is a sizable range of $H' < \kappa^{-1}$ for not large n_0. Using Eqs.(11) and (40), we integrated the PB equation in the region $0 < z - d_0 < H'$ for each given n_0 and σ_m. The parameters are those for silica oxide surfaces in Figs.11-16, but those for carboxyl-bearing surfaces are also used in Fig.17. For simplicity, we neglect the van der Waals interaction[1–3].

A. Results without applied field ($s = 0$)

First, we assume no applied field ($s = 0$). Because $dU/dz = 0$ at $z = H - d_H$, our H' corresponds to a half of the cell thickness in the symmetric case[15,22]. For thick cells with $H' > \kappa^{-1}$, it follows a well-known result[1,28,47],

$$\Pi_d \cong 64 T n_{\rm OH}^0 \exp(-2\kappa H'). \tag{70}$$

Ninham and Parsegian[15] derived the power-law behavior $\Pi_d \propto H^{-1/2}$ as $H \to 0$ between symmetric ionizable walls. From analysis in Appendix E, their asymptotic behavior appears for $H' \ll \ell_{\rm GC}$ in the case $A_1^{-1} \ll \alpha \ll 1$. Here, $\ell_{\rm GC} = (\kappa A_1 \alpha)^{-1}$ is the Gouy-Chapman length in Eq.(56) shorter than κ^{-1} in the nonlinear PB regime. The normalized potential values $U_0 = U(d_0)$ and $U_H = U(H - d_H)$ at the two ends are given by

$$U_H - U_0 \ \cong \ A_1 \alpha \kappa H' = H'/\ell_{\rm GC} \ll 1, \tag{71}$$
$$\exp(-U_0) \ \cong \ 4A_1 \alpha/\kappa H' \gg 1. \tag{72}$$

From Eq.(11) and (46), Π_d and α behave as

$$\Pi_d \cong T n_{\rm OH}^0 e^{-U_H} \cong T n_{\rm OH}^0 (\Gamma_0 K_s/K_{\rm w} H')^{1/2}, \tag{73}$$
$$\alpha \cong (K_s H'/\Gamma_0 K_{\rm w})^{1/2} n_{\rm OH}^0, \tag{74}$$

where we set $n_{\rm H}^0 = K_{\rm w}/n_{\rm OH}^0$. With other added ions, however, Eqs.(73) and (74) should be changed appropriately (see the comments below Eqs.(42) and (46))[15,22]. In addition, the inequality $\alpha \ll 1$ holds for

$$H' \ll (\Gamma_0/K_s)(K_{\rm w}^{1/2}/n_{\rm OH}^0)^2. \tag{75}$$

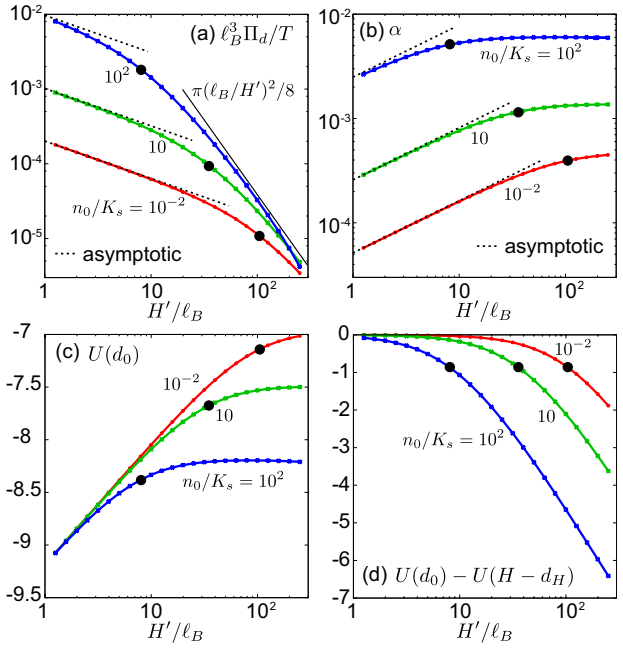

FIG. 11: Results for silica in the range $1 < H'/\ell_B < 300$ ($\ell_B = 7$ Å) without applied field ($s = 0$) for $n_0/K_s = 10^{-2}, 10$, and 10^2. Plotted are (a) $\ell_B^3\Pi_d/T$, (b) α, (c) $U(d_0)$, and (d) $U(d_0) - U(H - d_H)$. Points at which $H' = \ell_{\rm GC}$ are marked by • on each curve. In (a) and (b), formulae (73), (74), and (78) are written as guides of eyes. In (a)-(d), Eqs.(71)-(75) hold for $H' \ll \ell_{\rm GC}$ and Eqs.(76)-(78) for $H' \gg \ell_{\rm GC}$.

For silica oxide surfaces, we have $\Gamma_0/K_s \sim 10^8$ nm, so Eq.(76) can well be satisfied together with Eq.(71).

On the other hand, when $\ell_{\rm GC} \ll H' \ll \kappa^{-1}$ in the nonlinear PB regime, we find another regime (the Gouy-Chapman regime[28]), where U_0 and α remain nearly at constants but U_H strongly depends on H'. That is,

$$\exp(-U_0) \cong (2A_1\alpha)^2, \tag{76}$$
$$\exp(-U_H) \cong (\pi/\kappa H')^2. \tag{77}$$

Thus, $e^{U_H - U_0} \sim (H'/\ell_{\rm GC})^2 \gg 1$. The Π_d behaves as[28]

$$\Pi_d \cong T n_{\rm OH}^0 e^{-U_H} \cong \pi T/[2\ell_B(2H')^2], \tag{78}$$

which is independent of n_0 and α. In the previous theories[15,22], the behavior (78) was not found, because they adopted parameters yielding $\ell_{\rm GC} \gtrsim \kappa^{-1}$ with a salt added (see the last pragraph of Sec.IIIA).

In Fig.11, we show (a) Π_d, (b) α, (c) U_0, and (d) $U_0 - U_H$ as functions of H' in the range $\ell_B < H' < 300\ell_B < \kappa^{-1}$ without applied field ($s = 0$) for silica oxide surfaces. We set $n_0/K_s = 10^{-2}, 10$, and 10^2, where $\kappa\ell_B \times 10^3$ is 0.72, 1.6, and 5.0 and $A_1 \times 10^{-3}$ is 34, 15, and 4.9, respectively. In these cases, $A_1\alpha$ remains considerably larger than 1 for $H' > \ell_B = 7$ Å from Eq.(63). We can clearly see the crossover between the two power-law regimes at $H' = \ell_{\rm GC}$ as follows. In (a), Π_d behaves as in Eqs.(73) and (78). In (b), α decays as $\sqrt{H'}$ for small

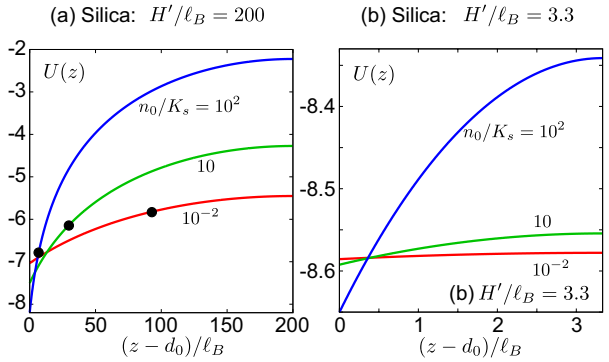

FIG. 12: Profiles of $U(z)$ in the range $0 < z - d_0 < H'$ for $s = 0$, where a silica oxide surface is at $z = 0$. For $n_0/K_s = 10^{-2}, 10$, and 10^2, H' is (a) $200\ell_B$ with $\ell_{\rm GC} < H' < \kappa^{-1}$ and is (b) $3.3\ell_B$ with $H' < \ell_{\rm GC}$.

H' and is a small constant for larger H'. In (c), U_0 satisfies Eqs.(72) and (76) in the range $[-9, -7]$, tending to be independent of n_0 for $H' \ll \ell_{\rm GC}$. In (d), $U_0 - U_H$ behaves in accord with Eqs.(71) and (77).

In Fig.12, we display $U(z)$ without applied field for $n_0/K_s = 10^{-2}, 10$, and 10^2. In (a), we set $H' = 200\ell_B < \kappa^{-1}$; then, $H' > \ell_{\rm GC}$ with $\ell_{\rm GC}/\ell_B = 6.7$, 30, and 93, respectively. In (b), we set $H' = 3.3\ell_B$ to realize $H' < \ell_{\rm GC}$ with $\ell_{\rm GC}/\ell_B = 440$, 87, and 10, where the diffuse layers at the bottom and top walls largely overlap,

B. Results with applied field

Next, we apply electric field by varying $s = \sigma_m/e\Gamma_0$ for $\kappa H' < 1$. In Fig.13, Π_d is displayed as a function of H' and s. We fix n_0/K_s at 10 and 10^3, where A_1 is 1.5×10^4 and 1.5×10^3, respectively. The Π_d is positive around the line of $s = 0$ but is mostly negative. This is natural because the surface charge densities at the two ends have the same sign only for $0 < s < \alpha$. If $\kappa H' \ll 1$, we find[53] that $\Pi_d > 0$ holds only for $|s| \lesssim \alpha$, where α is the degree of ionization at $s = 0$. This width of s is of order $\alpha \sim 10^{-3}$ in (a) and 10^{-2} in (b) from Eq.(63). In addition, for not small $|s|$, Π_d drops to negative values with large amplitude with decreasing H' due to partial screening (see below).

In Fig.14, we plot α and $u = \alpha - s$ for $1 < H'/\ell_B < 10^2$ and $-0.2 < s < 1.2$, where $n_0/K_s = 10$ (left) and 10^3 (right). For $H' \gtrsim 5\ell_B$, α is nearly independent of H' in the upper panels and u is very small for $0 < s \lesssim 1$ in the bottom panels. Thus, the self-regulation (found for $H' \gg \kappa^{-1}$ in Sec.III) is operative even for small $H'(\gtrsim 5\ell_B)$. We also write the lines of $u = 0$ and $\pm(A_1 H'\kappa)^{-1}$. We have $H' > \ell_{\rm GC}$ outside them. These three lines are closely located because of large A_1, which is 1.5×10^4 (left) and 1.5×10^3 (right). Indeed, on the flat area in the left, we have $-0.01 < u < -0.001$ and $A_1|u| > 15$.

In Fig.15, we show typical profiles of U for $u < 0$ and $s > 0$ with $H' = 5\ell_B = 0.08/\kappa$, which exhibit a negative

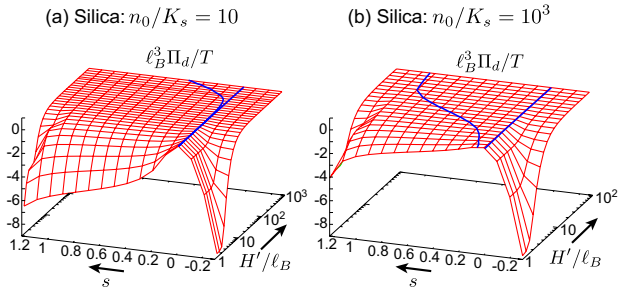

FIG. 13: $\ell_B^3\Pi_d/T$ in the H'/ℓ_B-s plane for small H' (silica), where n_0/K_s is (a) 10 and (b) 10^3. Lines of $\Pi_d = 0$ (blue) are written on the surfaces. Area of $\Pi_d > 0$ between the two lines becomes narrower as H' is decreased[53] but is widened as n_0 is incresaed. For relatively large s, Π_d drops to negative values with large amplitude due to partial screening.

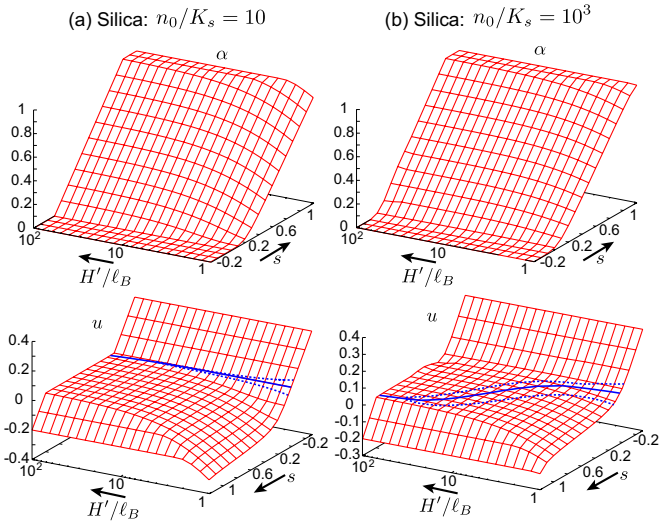

FIG. 14: α (top) and $u = \alpha - s$ (bottom) in the H'/ℓ_B-s plane for silica, where n_0/K_s is (a) 10 (left) and (b) 10^3 (right). For not small s (> 0), α is insensitive to H' larger than $5\ell_B$. Lines of $u = (A_1H')^{-1} > 0$, $u = 0$, and $u = -(A_1H')^{-1} < 0$ (from above) are written on the surfaces of u (blue lines). Below (above) the middle blue line ($u = 0$), u is negative (positive).

slope far from the walls. Such profiles can appear for $\Pi_d < 0$, so we define a dimensionless number b by

$$b = (-\Pi_d/2\pi T\ell_B)^{1/2}/\Gamma_0, \tag{79}$$

Then, $\Pi_d/Tn^0_{\rm OH} = -4A_1^2b^2$. The slope of U is $-2A_1b\kappa$ and the corresponding electric field is $4\pi e\Gamma_0 b/\varepsilon_0$ far from the walls. Here, the anions (OH^-) are accumulated at the bottom and the cations (M^+ and H^+) at the top, but their screening of the surface charges is only partial. The accumulated ion numbers $N_i = \int dz n_i(z)$ satisfy

$$N_{\rm OH} = \Gamma_0(|u| - b), \tag{80}$$
$$N_H + N_M = \Gamma_0(s - b), \tag{81}$$

which are consistent with Eq.(12). The degree of screening (screening fraction) is given by $1-b/|u|$ at the bottom

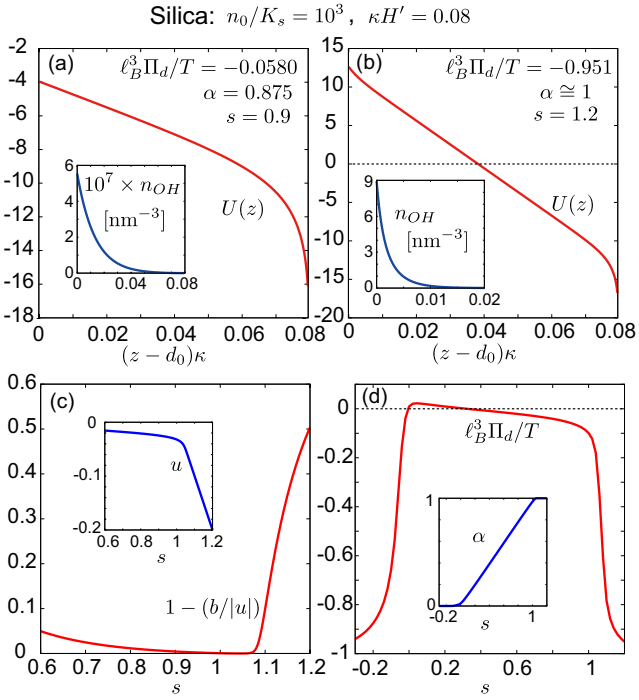

FIG. 15: Results for silica with $\kappa H' = 0.08$ and $n_0/K_s = 10^3$, where $\kappa = 2.2 \times 10^{-2}$/nm. Displayed is $U(z)$ in the range $0 < z - d_0 < H'$ for (a) $s = 0.9$, $\alpha = 0.875$, and $\ell_B^3\Pi_d/T = -0.0580$ and (b) $s = 1.2$, $\alpha = 1.0$, and $\ell_B^3\Pi_d/T = -0.951$. Plotted also is $n_{\rm OH}(z) = n^0_{\rm OH}e^{U(z)}$ near the bottom in units of nm^{-3} (inset). (c) Screening fraction $1 - b/|u|$ and u (inset) vs s. Screening is very weak for $s < 1.1$. (d) $\ell_B^3\Pi_d/T$ and α (inset) vs s, where $\Pi_d < 0$ for most s.

and by $1 - b/s$ at the top. It is 0 with no screening (with no diffuse layer) and is 1 for complete screening.

In Fig.15, at $n_0/K_s = 10^3$, we find $s = 0.9$, $\alpha = 0.875$, and $b = 0.0245 = 37/A_1$ in (a) and $s = 1.2$, $\alpha = 1.0$, and $b = 0.099 = 150/A_1$ in (b). Thus, $1 - b/|u|$ is 0.02 in (a) and 0.5 in (b). In fact, $n_{\rm OH}(z)$ is very small in (a) but is appreciable in (b) (inset). In (c), we show $1 - b/|u|$ vs s in the range $0.6 < s < 1.2$, which is very small for $s < 1.1$ but grows abruptly for $s > 1.1$. For $s < 1.1$, there is almost no screening at the bottom and the screening fraction at the top is α/s. In (d), we plot Π_d and α in the range $-0.2 < s < 1.2$, In accord with Fig.13, Π_d is positive only in a narrow range of s ($\lesssim \alpha \sim 10^{-2}$). Here u is negative and H' is small, but self-regulation behavior $|u| \ll 1$ in the range $0 < s < 1$ still persists.

The region of $\Pi_d > 0$ is widened with increasing n_0. See the two panels in Fig.13, where $n_0/K_s = 10$ and 10^3. In Fig.16, this is more apparent for $n_0/K_s = 10^4$ with $H' = 5\ell_B = 0.25\kappa^{-1}$, where $n^0_{\rm M} \cong n^0_{\rm OH} \gg n^0_{\rm H}$. In (a), Π_d is about $0.05T\ell_B^{-3} \sim 250Tn^0_{\rm OH}$ for $0 < s < 1$, where $U(z)$ is negative with a maximum about -6.0 and the ions in the cell are mostly M^+. However, Π_d becomes negative abruptly for $s > 1$. In (b), the profile of $U(z)$ exhibits a changeover across $s = 1$ at this n_0. For $s = 0.4$, E vanishes at the maximum point. However,

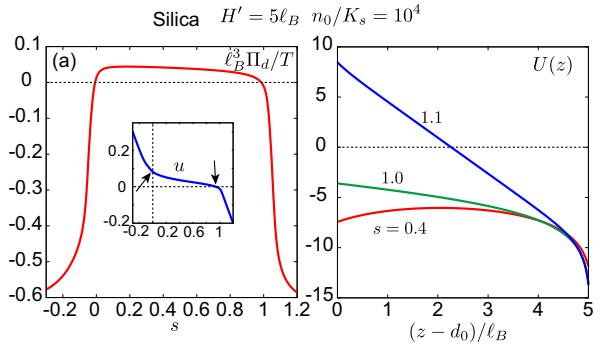

FIG. 16: (a) $\ell_B^3\Pi_d/T$ vs s in a cell with $H' = 5\ell_B = 0.25\kappa^{-1}$ for $n_0/K_s = 10^4$. For $0 < s < 1$, it is positive and is of order 0.05 with small positive $u = \alpha - s$ (inset). Point of $\Pi_d = 0$ are marked by arrows. (b) Profiles of $U(z)$ for $s = 0.4$, 1, and 1.1.

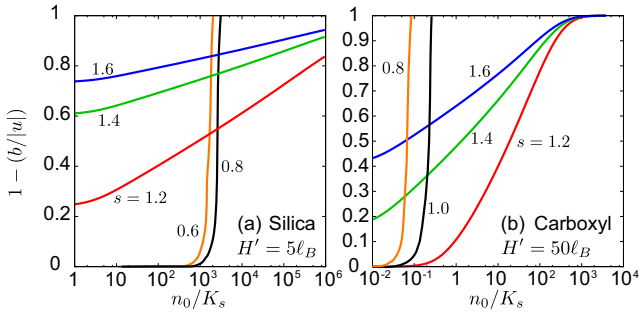

FIG. 17: Screening fraction $1 - b/|u|$ vs n_0/K_s at the bottom for (a) silica oxide surfaces with $H' = 5\ell_B$ and (b) carboxyl-bearing surfaces with $H' = 50\ell_B$ for five values of $s = \sigma_m/e\Gamma_0$. Screening increases with increasing n_0 and/or s. Changeover from unscreeing to screening is gradual for $s > 1$ but is abrupt for $0 < s < 1$.

once $\Pi_d < 0$, unscreening is significant at the bottom; in fact, $(u, 1 - b/|u|) = (-0.012, 0.10)$ for $s = 1.0$ and $(-0.10, 0.24)$ for $s = 1.1$. The charcteristic features of these behaviors are unchanged even for $n_0/K_s = 10^5$.

The screeing should be easier for larger n_0. This is confirmed in Fig.17, where plotted is $1 - b/|u|$ vs n_0/K_s at fixed s for (a) silica oxide surfaces and (b) carboxyl-bearing surfaces. Here, H' is $5\ell_B$ in (a) and is $50\ell_B$ in (b). The K_s and Γ_0 in the two systems are very different in Eqs.(15) and (67). Nevertheless, we can see significant unscreening at relatively small n_0 in the two systems. In addition, the changeover from unscreening to screening with increasing n_0 is nearly discontinuous for $0 < s < 1$ (from $b \cong s - \alpha$ to $b \cong 0$), while it is gradual for $s > 1$.

C. Theory of partial screening in thin cells

We finally present some analytic results on the partial screening. See Appendix E for their derivations. With $b \gg A_1^{-1}$, we introduce a characteristic length ℓ_∞ by

$$\ell_\infty = (2A_1 b)^{-1}\kappa^{-1} = (4\pi\ell_B\Gamma_0 b)^{-1}, \tag{82}$$

which is of the same order as $\ell_{\rm GC}$ in Eq.(56) for $|u| \sim b$. If we assume $U(H - d_H) = U_H < 0$ and $|U_H| \gg 1$, $U(z)$ near the top is well approximated by

$$U(z) \cong U_H + w + 2\ln(1 + a_H - a_H e^{-w}) \quad \text{(top)}, \tag{83}$$

where $w = (H - d_H - z)/\ell_\infty$ and $a_H = s/2b - 1/2$. The last term is zero at $w = 0$ and tends to $2\ln(1 + a_H)$ for $w \gg 1$, so the profile changes on the scale of ℓ_∞. This formula excellently describes the profiles in (a) and (b) of Fig.15 and those in Fig.16b near the top. The interior electric field is a constant for $\ell_\infty \ll H'$. For the profiles in Fig.15a and those of $s = 1$ and 1.1 in Fig.16b, we have $b \cong |u|$, so Eq.(83) can be used even at the bottom.

For the profile in Fig.15b, the diffusive layer near the bottom gives $b \cong 0.5|u|$. In this partial screening, the profile at the bottom is well approximated by

$$U(z) \cong U_0 - s - 2\ln(1 + a_0 - a_0 e^{-s}) \quad \text{(bottom)}, \tag{84}$$

where $U(d_0) = U_0 \gg 1$, $s = (z - d_0)/\ell_\infty$, and $a_0 = |u|/2b - 1/2$. For the profile in Fig.15b, Eqs.(83) and (84) should coincide far from the walls, so we require

$$\begin{aligned} H'/\ell_\infty &\cong U_0 - U_H - 2\ln[(1 + a_0)(1 + a_H)] \\ &\cong 4\ln(4A_1 b) + \ln\left[\frac{(|u| - b)(s - b)}{(|u| + b)(s + b)}\right] \end{aligned} \tag{85}$$

The right hand side can much exceed 1 for $A_1 b \gg 1$. For (b) in Fig.15, Eq.(85) is nearly exact.

VI. SUMMARY AND REMARKS

We have examined ionization on a dielectric film in water in applied field. In the geometry in Fig.1, the surface can be negatively charged with proton desorption. From the mass action law, the degree of dissociation α is determined by the ratio of the proton density close to the film $n_{\rm H}(0)$ and the dissociation constant $K_s (= 10^{-\rm pK}{\rm mol/L})$. We have added NaOH at a density n_0 in water[26] to decrease $n_{\rm H}(0)$. Main results are summarized as follows.

(i) In Sec.II, we have presented the free energy F, depending on the solute densities n_i and the degree of ionization α, where the the electrode charge density σ_m or the potential difference V is fixed. The contributions from the ionizable film and the Stern layers have been included. Minimization of the corresponding grand potential Ω yields equilibrium conditions including the mass action laws. The derivative of the equilibrium Ω with respect to the cell width H yields the osmotic pressure Π.

(ii) In Sec.III, we have assumed $H \gg \kappa^{-1}$. Analysis has been made on silica oxide films with pK= 7.3 in the nonlinear PB regime, where the Gouy-Chapman length $\ell_{\rm GC}$ is shorter than κ^{-1}. We have obtained a simple

equation for α in Eq.(61) for given σ_m and n_0. As in Fig.7b, we have found remarkable self-regulation behavior $\alpha \cong s = \sigma_m/e\Gamma_0$ for $0 < s < 1$ and $n_0 \ll n_c$, where Γ_0 is the areal density of the ionizable groups and n_c is a crossover density. From Eq.(62), we find $n_c = 10^{-2}$ mol/L for silica oxide surfaces.

(iii) In Sec.IV, we have presented results using the parameters of carboxyl-bearing surfaces with pK= 4.9. General trends are common to those for slica oxcide surfaces as in Figs.8 and 9, but numerical factors are very different. For example, we have $n_c = 2 \times 10^{-5}$ mol/L.

(iv) In Sec.V, we have presented analysis for small $H' = H - (d_0 + d_H)$ with a reservoir attached. Without applied field, the disjoining pressure Π_d is proportional to $\sqrt{H'}$ for $H' < \ell_{\rm GC}$ and to $(H')^{-2}$ for $\ell_{\rm GC} < H' < \kappa^{-1}$. In applied field, the self-regulation ($\alpha \cong s$ for $0 < s < 1$) holds even for $\ell_B < H' < \kappa^{-1}$. We have also found that the surface charges can be screened only partially for not small s. For silica oxide srfaces, Π_d is mostly negative for $n_0/K_s \lesssim 10^3$ in Figs.13 and 15(d), but it assumes a large positive value in the range $0 < s < 1$ for $n_0/K_s = 10^4$ in Fig.16. Similar results follow for hydroxyl-bearing surfaces as in Fig.17. We have derived analytic expressions for the potential profiles in partial screening.

(v) In Appendix A, we have examined the experimental method of imposing the fixed charge condition. In Appendix C, we have derived the expressions for the osmotic and disjoining pressures. In Appendix D, we have derived the expressions for the surface free energy for ionizable surfaces in applied field.

We make some remarks.

(1) There are a variety of ionizable surfaces with very different parameters (K_s and Γ_0)[14,17–21] under strong influence of ions. We have examined dissociation with small K_s, where the autoionization of water comes into play. The charge regulation has been controlled by the amount of NaOH. If K_s is much larger, we may add HCl to increase the bulk proton density $n_{\rm H}^0$. We can also add KCl to increase κ, as discussed below Eqs.(42), (46), and (74).

(2) In future we should study dynamics of surface ionization in nonstationary electric field. We note that the deprotonation on a silica-water interface takes place very slowly as rare thermal activations[54].

(3) There are a number of nonequilibrium situations with chemical reactions[27,55], where phase changes can take place. For example, elelectrowetting[49,50] has been studied without chemical reactions.

Acknowledgments

This work was supported by KAKENHI No.25610122. RO acknowledges support from the Grant-in-Aid for Scientific Research on Innovative Areas Fluctuation and Structure (Grant No. 25103010) from the Ministry of Education, Culture, Sports, Science, and Technology of Japan. We would like to thank Junpei Yamanaka for valuable discussions.

Appendix A: Realization of constant charge boundary condition

In Fig.1, a battery has been used to produce an equilibrium electrolyte state at a given potential difference V. If it is disconnected, the surface charge density σ_m (at the lower metal surface) becomes fixed.

As illustrated in Fig.1, we further connect a small external condenser with a capacitance $\mathcal{C}_{\rm ex}$ to the electrodes. The potential difference of the capacitor is given by

$$V_{\rm ex} = Q_{\rm ex}/\mathcal{C}_{\rm ex} \tag{A1}$$

where $Q_{\rm ex}$ is the initial charge. After this connection, the surface charge density and the potential difference of the electrodes are changed as $\sigma_m \to \sigma_m + \Delta\sigma_m$ and $V \to V + \Delta V$. Then, the capacitor change is changed by $-S_0\Delta\sigma_m$, where S_0 is the surface area of the electrodes. If the potential equilibration is attained, we have

$$V + \Delta V = [Q_{\rm ex} - S_0\Delta\sigma_m]/\mathcal{C}_{\rm ex} \tag{A2}$$

In the limit of small $\Delta\sigma_m$, we may set $\Delta V = \Delta\sigma_m/C_{\rm diff}$, where $C_{\rm diff} = \partial\sigma_m/\partial V$ is the differential capacitance of our system (per unit area). Then, Eq.(A2) yields

$$\begin{aligned}\Delta\sigma_m &= (V_{\rm ex} - V)/[S_0/\mathcal{C}_{\rm ex} + 1/C_{\rm diff}] \\ &\cong (V_{\rm ex} - V)\mathcal{C}_{\rm ex}/S_0,\end{aligned} \tag{A3}$$

where the second line holds for $C_{\rm ex} \ll S_0 C_{\rm diff}$. Therefore, for sufficiently small $\mathcal{C}_{\rm ex}$, $\Delta\sigma_m$ depends only on the initial V of our system and remains fixed independently of the subsequent physical and chemical processes in the cell.

Appendix B: Bulk ion densities in terms of $n_{\rm MOH}$

In Eq.(40) we can assume the relation,

$$n_{\rm M}^0 + n_{\rm H}^0 = n_{\rm OH}^0, \tag{B1}$$

without loss of generality by shifting the origin of $U(z)$ appropriately ($U \to U +$ constant). Then, we obtain Eq.(41). From the chemical equilibrium conditions (4) and (5), $n_{\rm H}^0$ and $n_{\rm M}^0$ are expressed as

$$n_{\rm H}^0 = K_{\rm w}/n_{\rm OH}^0, \quad n_{\rm M}^0 = K_{\rm b} n_{\rm MOH}/n_{\rm OH}^0. \tag{B2}$$

From Eqs.(B1) and (B2) $n_{\rm OH}^0$ is given by

$$n_{\rm OH}^0 = (K_{\rm w} + K_{\rm b} n_{\rm MOH})^{1/2}. \tag{B3}$$

The density n_0 of M atoms in Eq.(7) is expressed as

$$n_0 = n_{\rm MOH}(1 + K_{\rm b}/n_{\rm OH}^0). \tag{B4}$$

For $\kappa H \gg 1$, n_i^0 coincide with those in Eqs.(6)-(8).

We can attach a reservoir with the same $n_{\rm MOH}$ as that in the cell. Then, the reservoir densities of $\rm H^+$, $\rm OH^-$, and $\rm M^+$ are given by $n_{\rm H}^0$ and $n_{\rm OH}^0$, and $n_{\rm M}^0$ in Eqs.(B2) and (B3). The reservoir osmotic pressure is written as

$$\Pi_r^0 = T\sum_i n_i^0 = T(n_{\rm MOH} + 2n_{\rm OH}^0). \tag{B5}$$

Appendix C: Force between parallel walls

We suppose two equilibrium states in the geometry in Fig.1, where the cell length is H in one state and $H+\delta H$ in the other slightly elongated one. The water density and the temperature are common. All the quantities are independent of the lateral coordinates x and y. The grand potentials Ω and Ω' per unit area are defined in the two states from Eq.(32) or Eq.(35). We calculate the difference $\delta\Omega = \Omega' - \Omega$ for small δH.

In the elongated state, the quantities are denoted with a prime and the space coordinate is written as z', where $n_i'(z')$ are the densities and α' is the degree of ionization. We impose $\sigma_m' = \sigma_m$ at fixed charge and $V' = V$ at fixed potential difference. We assume a mapping relation between the positions z' and z as[51,54]

$$z' = z + w(z), \tag{C1}$$

where $w(z)$ is a small *displacement* with $w(0) = 0$ and $w(H) = \delta H$. We consider the deviations,

$$\delta n_i = n_i'(z') - n_i(z), \quad \delta\alpha = \alpha' - \alpha. \tag{C2}$$

The mapping (C1) yields $d/dz = (1+w')d/dz'$ and $\int_0^{H+\delta H} dz' = \int_0^H dz(1+w')$, with $w' = dw/dz$. Then, from $\varepsilon_0 dE'/dz' = 4\pi\rho'(z')$, the deviation $\delta E = E'(z') - E(z)$ is related to $\delta\rho = \rho'(z') - \rho(z)$ as

$$\varepsilon_0 \frac{d}{dz}\delta E = 4\pi(w'\rho + \delta\rho), \tag{C3}$$

to linear order. From Eq.(23) the deviation in the electrostatic free energy, $\delta F_e = F_e' - F_e$, is calculated as

$$\begin{aligned}\delta F_e &= \int dz w'[\frac{\varepsilon_0}{8\pi}E^2 + \rho\Phi] \\ &+ \int dz\Phi\delta\rho + \Phi(0)\delta\sigma_{\rm A} + V\delta\sigma_m,\end{aligned} \tag{C4}$$

where the first term arises from the cell elongation and the other terms coincide with those in Eq.(24). Similarly, the elongation contribution to F_b in Eq.(26) is given by $\int dz w' f_b$, where f_b is the bulk free energy density in $F_b = \int dz f_b$. From Eq,(32) or Eq.(35), we find

$$\begin{aligned}\delta\Omega &= -\int dz w'\Pi - (N_{\rm M} + N_{\rm MOH})\delta h_0 \\ &= -\Pi\delta H - (N_{\rm M} + N_{\rm MOH})\delta h_0,\end{aligned} \tag{C5}$$

where $\delta h_0 = h_0' - h_0$ and Π is given in Eq.(44). Since Π is a constant, we obtain the second line. Note that Eq.(C5) holds both at fixed σ_m and fixed V.

The 1D theory in this appendix can be extended in various 3D situations. For example, we can calculate the solvent-mediated interaction between colloidal particles in a mixture solvent[51]. The 3D mapping $x_\alpha' = x_\alpha + w_\alpha$ has been used in elasticity theory. Moreover, we can use it to derive the stress tensor for various fluids (including near-critical fluids, liquid crystals, and electrolytes)[54].

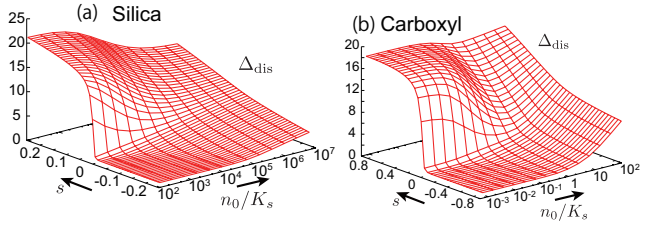

FIG. 18: Normalized decrease in the dissociation free energy per ionized group $\Delta_{\rm dis}$ in Eq.(D5) in the s-n_0/K_s plane for (a) silica and (b) carboxyl-bearing interfaces. These are calculated from the grand potential Ω in the limit $H \gg \kappa^{-1}$.

Appendix D: Calculation of surface free energy

We calculate Ω in Eq.(35) at fixed σ_m and $n_{\rm OH}^0$ using Eqs.(18), (33), and (34). It is rewritten as

$$\begin{aligned}\Omega = &-\int dz\Big[T\sum_i n_i + \frac{\varepsilon_0}{8\pi}E^2\Big] - \frac{\sigma_A^2}{2C_O} + \frac{\sigma_m^2}{2C_{\rm tot}} + F_s \\ &+T\Gamma_0\alpha\ln[n_{\rm H}(0)\lambda_{\rm H}^3] + [\Phi(d_0) - \Phi(H-d_H)]\sigma_m\end{aligned} \tag{D1}$$

where $C_{\rm tot}^{-1} = C_0^{-1} + C_H^{-1} + C_d^{-1}$. At fixed V, we should subtract $V\sigma_m$ from the right hand side.

We assume a thick cell with $\kappa H \gg 1$, where $n_i \to n_i^0$ and $E \to 0$ far from the walls. Then, using Eqs.(40) and (47), we can rewrite Eq.(D1) as

$$\Omega = -H\Pi_r^0 + \gamma_H + \gamma_0 + \sigma_m^2/2C_{\rm tot}. \tag{D2}$$

where Π_r^0 is the reservoir osmotic pressure in Eq.(B5). The γ_H is the surface free energy from the upper diffuse layer (without surface ionization) given by

$$\gamma_H/T = [1 - (A_1^2s^2+1)^{1/2}]\kappa/\pi\ell_B + g(A_1s)\sigma_m/e, \tag{D3}$$

where $g(x) = 2\ln[\sqrt{1+x^2}+x]$. The γ_0 is that of the lower surface and the difference $\Delta\Omega = \gamma_0 - \gamma_H$ is the contribution due to the surface ionization of the form,

$$\begin{aligned}\frac{\Delta\Omega}{T\Gamma_0} = &\frac{2}{A_1}[(A_1^2s^2+1)^{1/2} - (A_1^2u^2+1)^{1/2}] + \frac{F_s}{T\Gamma_0} \\ &+\alpha\ln[n_{\rm H}(0)\lambda_{\rm H}^3] - s[g(A_1u) + g(A_1s)] - \frac{A_2}{2}\alpha^2.\end{aligned} \tag{D4}$$

The above $\Delta\Omega$ coincides with $\Delta\Omega$ in Fig.5 calculated from integration of $d\Omega/d\alpha$ in Eq.(36). In fact, differentiation of Eq.(D4) with respect to α at fixed s yields Eq.(36), since $\partial[\ln[n_{\rm H}(0)]/\partial\alpha = A_2 + 2A_1(1+A_1^2u^2)^{-1/2}$ from Eq.(59). In chemical equilibrium (11), α and $\Delta\Omega$ are functions of s and n_0, where $F_s/T\Gamma_0 + \alpha\ln[n_{\rm H}(0)\lambda_{\rm H}^3] = \ln(1-\alpha) = -\ln[1+K_s/n_{\rm H}(0)]$ in Eq.(D4). We define

$$\Delta_{\rm dis} = -\Delta\Omega/T\Gamma_0\alpha, \tag{D5}$$

in equilibrium. Then, $-T\Delta_{\rm dis}$ is the dissociation free energy per ionized group, including the effects of the diffusive and Stern layers and the electrode. In Fig.18, we

display $\Delta_{\rm dis}$. For $n_0 < n_c$, it is close to 1 for $\alpha \ll 1$ (for $s < 0$) but it is 10-20 for not small α (for $s > 0$). For $n_0 > n_c$, it increases gradually with increasing s.

Appendix E: Calculations for thin cells

Calculations for $s = 0$. We first present analysis in the relatively simple case of $s = 0$ for $A_1\alpha \gg 1$, where $U(z) < 0$ with large $|U|$. Since dU/dz is equal to 0 at $z = H - d_H$ and to $2\kappa A_1\alpha$ at $z = d_0$, Eq.(46) yields

$$\kappa^{-2}(dU/dz)^2 \cong e^{-U(z)} - e^{-U_H}, \tag{E1}$$

$$(2A_1\alpha)^2 \cong e^{-U_0} - e^{-U_H}, \tag{E2}$$

We can integrate Eq.(E1) in the following form,

$$\kappa(H - d_H - z) \cong 2e^{U_H/2}\tan^{-1}(\sqrt{q(z)}), \tag{E3}$$

where we use $\int_0^x dy(1/\sqrt{e^y - 1}) = 2\tan^{-1}(\sqrt{e^x - 1})$ by setting $y = U_H - U$. We define

$$q(z) = \exp[U_H - U(z)] - 1. \tag{E4}$$

where $q(H - d_H) = 0$ and $q(d_0) = (2A_1\alpha)^2\exp(U_H)$. There are two cases. If $q \ll 1$, we can set $\tan^{-1}\sqrt{q} \cong (U_H - U)^{1/2} \ll 1$ in Eq.(E3) to obtain $H' \ll \ell_{\rm GC}$ and Eqs.(71)-(74). On the other hand, if $q \gg 1$, we can set $\tan^{-1}\sqrt{q} \cong \pi/2$ to obtain $H' \gg \ell_{\rm GC}$ and Eqs.(76)-(78).

Calculations of partial screening. We explain the partial screening in Fig.15 with $s > 0$ and $u < 0$. In terms of b in Eq.(79), the PB equation in Eq.(46) becomes

$$2\cosh(U) - 2 = \kappa^{-2}(dU/dz)^2 - (2A_1 b)^2. \tag{E5}$$

At $z = d_0$ and $H - d_H$, we find

$$\cosh(U_0) - 1 = 2A_1^2(u^2 - b^2), \tag{E6}$$

$$\cosh(U_H) - 1 = 2A_1^2(s^2 - b^2), \tag{E7}$$

If $U_H < 0$ and $|U_H| \gg 1$, we can replace $\cosh(U) - 1$ by $e^{-U}/2$ in Eq.(E5) near the top. It follows Eq.(83). Integration of $n_{\rm H}(z)/n_{\rm H}^0 = n_{\rm M}(z)/n_{\rm M}^0 = e^{-U}$ near the top can be performed to give Eq.(81). On the other hand, if $U_0 \gg 1$, we can replace $\cosh(U) - 1$ by $e^U/2$ near the bottom. Then, Eq.(84) is obtained and integration of $n_{\rm OH}(z)/n_{\rm OH}^0 = e^U$ near the bottom yields Eq.(80).

[1] J. N. Israelachvili, *Intermolecular and Surface Forces* (Academic Press, London, 1991).

[2] R. J. Hunter, Foundations of Colloid Science (Oxford University Press, Oxford, 2001). See Chap.10 in this book.

[3] H.-J. Butt, K. Graf, and M. Kappl, Physics and Chemistry of Interfaces, 3rd ed. (Wiley-VCH Verlag GmbH, Weinheim, 2013).

[4] D. Ben-Yaakov, D. Andelman, R. Podgornik, D. Harries, Current Opinion in Colloid and Interface Science **16**, 542 (2011).

[5] T. W. Healy and D. W. Fuerstenau, J. Colloid Sci. **20**, 376 (1965).

[6] J. Westall and H. Hohl, Adv. Colloid Interface Sci. **12**, 265 (1980).

[7] T. Hiemstra, J. C. M. de Wit, and W. H. van Riemsdijk, J. Colloid Interface Sci. **133**, 105 (1989).

[8] K. F. Hayes, G. Redden, W. Ela, and J. O. Leckie, J. Colloid and Interf. Sci. **142**, 448 (1991).

[9] J. J. Sonnefeld, J. Colloid Interface Sci. **155**, 191 (1993).

[10] R.E.G. van Hal, J.C.T. Eijkel, and P. Bergveld, Adv. Colloid Interface Sci.**69**, 31 (1996).

[11] J. N. Israelachvili and R. M. Pashley, J. of Colloid and Interface Science, **98**, 500 (1984).

[12] A. Grabbe, Langmuir **9**, 797 (1993).

[13] C. Zhao, D. Ebeling, I. Siretanu, D. van den Ende, and F. Mugele, Nanoscale **7**, 16298 (2015).

[14] G. Trefalt, S. H. Behrens, and M. Borkovec, Langmuir **32**, 380 (2016).

[15] B. W. Ninham and V. A. Parsegian, J. Theor. Biol. **31**, 405428 (1971).

[16] D. Y. C. Chan, T. W. Healy, and L. R. White, J. Chem. Soc., Faraday Trans. I, **172**, 2844 (1976).

[17] S. H. Behrens and M. Borkovec, J. Phys. Chem. B **103**, 2918 (1999); Phys. Rev. E **60**, 7040 (1999).

[18] S. H. Behrens, D. Iso Christl, R. Emmerzael, P. Schurtenberger, and M. Borkovec Langmuir **16**, 2566 (2000).

[19] S. H. Behrens and D.G. Grier, J. Chem. Phys. **2001**, **115**, 6716 (2001).

[20] P. W. Biesheuvel and W. B. S. de Lint, J. Colloid Interface Sci. **241**, 422 (2001); P. M. Biesheuvel, Langmuir **17**, 3553 (2001).

[21] M. Heinen, T. Palberg, and H. Löwen J. Chem. Phys. **140**, 124904 (2014)

[22] T. Markovich, D. Andelman, and R. Podgornik, EPL, **113** ,26004 (2016). Their expression for Π_d in the Ninham-Parsegian regime is obtained if $n_{\rm OH}^0/n_{\rm H}^0 = (n_{\rm OH}^0)^2/K_{\rm w}$ in our expression in Eq.(73) is replaced by 1.

[23] M. Eigen and L. De Maeyer, Z. Elektrochem. **59**, 986 (1955); M. Eigen and L. De Maeyer, Proc. Roy. Soc. (London), Ser. A **247**, 505 (1958).

[24] T. Gisler, S. F. Schulz, M. Borkovec, H. Sticher, P. Schurtenberger, B. D'Aguanno, and R. Klein, J. Chem. Phys. **101**, 9924 (1994).

[25] R. Pericet-Camara, G. Papastavrou, S. H. Behrens, and M. Borkovec, J. Phys. Chem. B **108**, 19467 (2004).

[26] J. Yamanaka, Y. Hayashi, N. Ise, and T. Yamaguchi, Phys. Rev. E **55**, 3028 (1997).

[27] M. Murai, H. Yamada, J. Yamanaka, S. Onda, M. Yonese, K. Ito, T. Sawada, F. Uchida, and Y. Ohki, Langmuir **23**, 7510 (2007).

[28] D. Andelman, *Introduction to Electrostatics in Soft and Biological Matter*. In Soft Condensed Matter Physics in Molecular and Cell Biology; Poon, W., Andelman, D., Eds.; Scottish Graduate Series; Taylor & Francis: New York, 2006; p 97.

[29] A. Onuki, R. Okamoto, and T. Araki, Bull. Chem. Soc.

Jpn. **84** (2011) 284113.
[30] R. Okamoto and A. Onuki, Phys. Rev. E **84**, 051401 (2011)
[31] E. Raphael and J. F. Joanny, Europhys. Lett. **13**, 623 (1990).
[32] I. Borukhov, D. Andelman, and H. Orland, Eur. Phys. J. B **5**, 869 (1998).
[33] Y. Burak and R. R. Netz, J. Phys. Chem. B **108**, 4840 (2004)
[34] R. Okamoto and A. Onuki, J. Chem. Phys. **131**, 094905 (2009).
[35] A. Onuki and R. Okamoto, J. Phys. Chem. B **113**, 3988 (2009).
[36] M. Muthukumar, J. Chem. Phys. **120**, 9343 (2004); M. Muthukumar, J. Hua, and A. Kundagrami, J. Chem. Phys. **132**, 084901 (2010).
[37] G. S. Longo, M. O. de la Cruz, and I. Szleifer, Soft Matter, **8**, 1344 (2012).
[38] T. Araki, Soft Matter, **12**, 6111 (2016).
[39] C. B. Post and B. H. Zimm, Biopolymers 21, 2139 (1982); . P. G. Arscott, C. Ma, J. R. Wenner, and V. A. Bloomfield, Biopolymers 36, 345 (1995); A. Hultgren and D. C. Rau, Biochemistry 43, 8272 (2004); C. Stanley and D. C. Rauy, Biophys. J. 91, 912 (2006).
[40] D. M. Kolb, Surf. Sci., **500**, 722 (2002).
[41] J. Hautman, J. W. Halley, and Y.-J. Rhee, J. Chem. Phys. 91, 467 (1989).
[42] I.-C. Yeh and M.L. Berkowitz, J. Chem. Phys. 111, 3155 (1999).
[43] P. S. Crozier, R. L. Rowley, and D. Henderson, J. Chem. Phys. **113**, 9202 (2000).
[44] A. P.Willard, S. K. Reed, P. A. Madden, and D. Chandler, Faraday Discuss. **141**, 423 (2009).
[45] K. Takae and A. Onuki, J. Phys. Chem. B **119**, 9377 (2015); J. Chem. Phys. **143**, 154503 (2015)
[46] As the Stern potential drop, we find the expression $V_0^{\rm S} = 4\pi \int_0^{d_0} dz[P_b - P(z)]$, where $P_b = (\varepsilon_0 - 1)E(d_0)/4\pi$ is the bulk polarization close to the bottom Stern layer[45].
[47] H. Ohshima, *Theory of Colloid and Interfacial Electric Phenomena* (Elsevier, New York, 2006).
[48] L. D. Landau and E. M. Lifshitz, Electrodynamics of Continuous Media (Pergamon, New York, 1984), Vol. 8.
[49] D. Klarman and D. Andelman, Langmuir **27**, 6031 (2011).
[50] F. Mugele and J.C. Baret, J. Phys.: Cond. Mat. **17**, R705 (2005).
[51] R. Okamoto and A. Onuki, Phys. Rev. E **88**, 022309 (2013).
[52] K. Aoki, T. Li, J. Chen, and T. Nishiumi, J. Electroanal. Chem. **613**, 1 (2008); K. Aoki, T. Li, J. Chen, and T. Nishiumi, J. Electroanal. Chem. **633**, 319 (2009).
[53] Setting $\Pi_d = 0$, we solve Eq.(41) for $u < 0$ and $s > 0$ exactly as $\tanh(U/4) = -C\exp[\kappa(z - d_0)]$. For $A_1|u| \gg 1$ we have $C \cong 1 + 1/A_1|u|$ and $s(|u| - \alpha) \cong \alpha/2A_1\kappa H'$. Then, $s \cong \alpha$ for $H' > 1/A_1\alpha\kappa = \ell_{\rm GC}$.
[54] A. Onuki, *Phase Transition Dynamics* (Cambridge University Press, Cambridge, 2002). See Appendix 6A in this book.
[55] M. Z. Bazant, M. S. Kilic, B. D. Storey, and A. Ajdari, Adv. Colloid Interface Sci. **152**, 48 (2009).